THE ASTROPHYSICAL JOURNAL SUPPLEMENT SERIES, 98:103–128, 1995 May

ULTRAVIOLET TO NEAR-INFRARED SPECTRAL DISTRIBUTIONS OF STAR-FORMING AND SEYFERT 2 GALAXIES

THAISA STORCHI-BERGMANN[1]
Departamento de Astronomia, IF-UFRGS, CP 15051, CEP 91501-970, Porto Alegre, RS, Brazil
ANNE L. KINNEY[1,2] AND PETER CHALLIS[1]
Space Telescope Science Institute, 3700 San Martin Drive, Baltimore, MD 21218
Received 1994 April 29; accepted 1994 July 14

ABSTRACT

Combined UV, optical, and near-IR spectral distributions of a sample of 48 southern star-forming and Seyfert 2 galaxies are presented. The optical and near-IR spectra were obtained using apertures matching those of the UV observations ($10'' \times 20''$) and in most cases correspond to the bulk of the gas and stellar population contribution from the whole galaxy. No such data set—taken with matched apertures and spanning such a large spectral range—exists in the literature today. The obtained spectral distributions are particularly useful as a comparison sample for spectroscopic surveys of more distant galaxies. Emission-line fluxes, continuum fluxes, and equivalent widths of absorption lines are measured from the spectra, and average values corresponding to the different activity types—blue compact dwarf, blue compact, starburst, Seyfert, and composite (starburst and Seyfert)—are presented and discussed.

Subject headings: galaxies: Seyfert — galaxies: starburst — galaxies: photometry — infrared: galaxies — ultraviolet: galaxies

1. INTRODUCTION

In a previous work, Kinney et al. (1993) have produced an atlas of ultraviolet spectra of the central regions of 143 galaxies showing star formation in its nucleus, from observations obtained with the *IUE* satellite. In order to extend the spectral distributions to the optical and near-IR, ground-based observations have been made using a matched aperture to that of the UV ($10'' \times 20''$). In this work we present the data of the southern sample, obtained at the Cerro Tololo Inter-American Observatory (CTIO). With these observations we were able to construct spectral distributions from 1200 to 10,000 Å, with an average spectral resolution of 5 Å for 48 star-forming and Seyfert 2 galaxies. Optical spectra of the northern sample were obtained at the Kitt Peak National Observatory and will be presented in McQuade, Calzetti, & Kinney (1995).

In this work we also provide measurements of emission-line fluxes and equivalent widths of the absorption lines, as well as fluxes at several points of the continuum for the southern sample, which were used to determine the chemical abundance, reddening, star-forming rate, and age of the central regions of the sample galaxies. The study of the dependence of the spectral distributions on the above parameters, for both the southern and northern sample, are presented in two other papers (Storchi-Bergmann, Calzetti, & Kinney 1994; Calzetti, Kinney, & Storchi-Bergmann 1994). Galaxies with similar properties are being grouped together in order to construct template spectra (Kinney, Calzetti, & Storchi-Bergmann 1995). Our goal is to understand the star formation in nearby galaxies and to use the results of our study to predict the properties of star-forming galaxies at high redshift. The large aperture of our observations usually includes most of the galaxy light, so that our spectral distributions are well suited for comparison with observations of distant galaxies, for which even small apertures include most of the galaxy.

2. OBSERVATIONS

Long-slit spectral observations were made at CTIO in three epochs: 1991 October–November, 1992 May, and 1992 November. In order to get an aperture as close as possible to the one from *IUE* observations, we used a slit width corresponding to 10″ in the sky, and then extracted a window 20″ long. Two telescopes were used in the optical and near-IR observations: the 1 m telescope with Cassegrain Spectrograph and 2DFRUTTI detector was used to cover the range λλ3200–6400 with 8 Å resolution, and the 1.5 m telescope with Cassegrain Spectrograph and a CCD detector to cover the range λλ6400-10000 at 5.5 Å resolution. The spectral resolution was chosen to be as close as possible to the one of the UV observations, which are 5 Å for the SWP and 8 Å for the LWP and LWR. A log of the observations is presented in Table 1. The activity types and distances of the galaxies, obtained from Kinney et al. (1993, from the apparent B and absolute M_B magnitudes listed on their Table 1), are listed in the second and third columns of the table.

The spectra were reduced using the IRAF software, including flux calibration through observations of standard stars. The near-IR spectra were then corrected for the atmospheric absorption bands of H_2O and O_2 by dividing the galaxies' spectra by the spectra of hot standard stars, after removing the Hα absorption line when present in the stellar spectrum and normalizing the slope of the stellar continuum to 1. Two examples of the resulting spectral distributions are shown in Figures 1 (a typical blue spectrum) and 2 (a typical red spectrum).

[1] Visiting Astronomer at the Cerro Tololo Inter-American Observatory, operated by the Association of Universities for Research in Astronomy, Inc., under contract with the National Science Foundation.
[2] Guest investigator with *IUE* Observatory.

1995ApJS...98..103S

TABLE 1

LOG OF THE OBSERVATIONS

Galaxy	Activity Type	Dist. (Mpc)	Date	Spectral Range (A)	Exposure Time(s)	Comments
IC1586	BCG	121.9	11/06/92	6400–8200	900	
			11/07/92	8200–10000	1200	
Haro 15	BCG	130.0	11/07/91	3200–3700	1800	
			10/28/91	3700–6400	1800	
			11/06/92	6400–8200	900	
			11/08/92	8200–10000	1200	clouds
ESO296-11		114.3	11/03/92	3200–6400	3600	
			11/06/92	6400–8200	1200	
			11/07/92	8200–10000	1200	
NGC1068	Sy2	31.3	11/05/92	3200–6400	1800	λ5007 saturated
			11/08/92	6400–8200	300	clouds
			11/07/92	8200–10000	600	
NGC1097	Hs+Lin	31.1	11/06/91	3200–3700	900	
			10/30/91	3700–6400	1200	
			11/06/92	6400–8200	400	
			11/07/92	6400–10000	700	
NGC1140	BCG	43.9	11/03/92	3200–6400	3600	
			11/06/92	6400–8200	400	
			11/07/92	8200–10000	800	
NGC1313	HII	6.4	11/04/92	3200–6400	3600	
			11/06/92	6400–8200	500	
			11/07/92	8200–10000	1000	
NGC1433	Lin	23.2	11/06/91	3200–3700	900	
			11/01/91	3700–6400	1200	
			11/06/92	6400–8200	300	
			11/07/92	8200–10000	600	
NGC1510	BCDG	16.8	11/03/92	3200–6400	3600	
			11/06/92	6400–8200	900	
NGC1553		21.7	11/06/91	3200–3700	900	
			10/30/91	3700–6400	1200	
			11/06/92	6400–8200	300	
			11/07/92	8200–10000	600	
NGC1614	SB	110.2	11/03/92	3200–6400	3600	
			11/06/92	6400–8200	600	
			11/07/92	8200–10000	900	
NGC1672	SB+Sy	30.2	11/07/91	3200–3700	1200	
			10/30/91	3700–6400	1800	
			11/06/92	6400–8200	600	
			11/07/92	8200–10000	600	
NGC1667	Sy2	114.3	11/02/92	3200–6400	3000	
			11/06/92	6400–8200	600	
			11/07/92	8200–10000	700	
NGC1705	BCDG	9.1	11/06/91	3200–3700	870	
			11/01/91	3700–6400	1200	
			11/06/92	6400–8200	600	
			11/07/92	8200–10000	600	
NGC1800	HII	12.0	11/04/92	3200–6400	3600	
			11/06/92	6400–8200	600	
			11/07/92	8200–10000	1200	
NGC3049	SB	31.1	05/30/92	3200–6400	1800	
			05/19/92	6400–8200	900	
			05/20/92	8200–10000	600	
NGC3081	Sy2	46.8	11/08/91	3200–3700	1800	
			11/09/91	3700–6400	1500	
			05/19/92	6400–8200	300	
			05/20/92	8200–10000	450	
NGC3125	BCDG	18.4	11/08/91	3200–3700	1500	
			11/09/91	3700–6400	1200	
			05/19/92	6400–8200	300	
			05/20/92	8200–10000	600	
NGC3256	SB	90.4	05/30/92	3200–6400	1800	
			05/20/92	6400–8200	300	
			05/21/92	8200–10000	600	clouds
NGC3351	Hs	17.2	06/01/92	3200–6400	1800	
			05/20/92	6400–8200	300	
			05/21/92	8200–10000	600	
			05/22/92	8200–10000	300	
NGC3393	Sy2	86.7	05/31/92	3200–6400	1800	
			05/20/92	6400–8200	450	
			05/21/92	8200–10000	600	
			05/22/92	8200–10000	300	
1050+04	BCG	124.7	06/01/92	3200–6400	1800	
			05/20/92	6400–8200	600	clouds
			05/21/92	8200–10000	600	
			05/22/92	8200–10000	300	
NGC3660	Sy1/NELG	70.5	05/31/92	3200–6400	1800	
			05/20/92	6400–8200	300	clouds
			05/21/92	8200–10000	600	cirrus
			05/22/92	8200–10000	300	
ESO572-34	HII	21.2	05/31/92	3200–6400	1800	
			05/20/92	6400–8200	300	clouds
			05/24/92	8200–10000	600	
			05/22/92	8200–10000	1200	
NGC4385	SB	48.5	05/31/92	3200–6400	1800	
			05/20/92	6400–8200	300	clouds
			05/21/92	8200–10000	600	cirrus
			05/22/92	8200–10000	300	
NGC4569	Lin	32.2	06/01/92	3200–6400	1800	
			05/21/92	8200–10000	600	cirrus
			05/22/92	8200–10000	300	

TABLE 1—*Continued*

Galaxy	Activity Type	Dist. (Mpc)	Date	Spectral Range (A)	Exposure Time(s)	Comments
NGC4579	Lin	28.2	06/01/92	3200–6400	1800	
			05/21/92	8200–10000	300	cirrus
			05/22/92	8200–10000	300	
NGC4594	Lin	26.2	05/31/92	3200–6400	900	
			05/20/92	6400–8200	300	clouds
			05/21/92	8200–10000	600	cirrus
IC3639	Sy2	70.5	05/31/92	3200–6400	1800	
			05/20/92	6400–8200	300	clouds
			05/21/92	8200–10000	600	cirrus
			05/22/92	8200–10000	600	
NGC4748	Sy1	82.2	05/31/92	3200–6400	1800	
			05/20/92	6400–8200	300	clouds
			05/21/92	8200–10000	600	cirrus
			05/22/92	8200–10000	300	
NGC5102	SB	7.5	05/31/92	3200–6400	1500	
			05/20/92	6400–8200	300	clouds
			05/21/92	8200–10000	600	cirrus
			05/22/92	8200–10000	300	
NGC5135	Sy2	125.3	06/01/92	3200–6400	1800	haze
			05/20/92	6400–8200	300	clouds
			05/21/92	8200–10000	600	cirrus
			05/22/92	8200–10000	300	
NGC5236	SB	8.4	06/01/92	3200–6400	1800	haze
			05/20/92	6400–8200	300	clouds
			05/21/92	8200–10000	600	cirrus
			05/22/92	8200–10000	300	
NGC5253	BCG	7.3	06/01/92	3200–6400	1800	haze
			05/20/92	6400–8200	300	clouds
			05/21/92	8200–10000	600	cirrus
			05/22/92	8200–10000	300	
NGC5506	Sy2	45.5	05/31/92	3200–3700	1800	
			05/20/92	3700–7100	600	
			05/22/92	8200–10000	600	
NGC5643	Sy2	26.2	05/31/92	3200–3700	1800	
			06/29/92	3700–7100	1800	
			05/22/92	8200–10000	600	
NGC5728	Sy2	82.0	05/31/92	3200–5600	1800	
			07/01/92	5600–7100	1800	
			05/22/92	8200–10000	600	
NGC6221	SB+Sy2	41.1	05/31/92	3200–4800	1800	
			10/28/91	4800–6400	1200	
			05/20/92	6400–8200	600	clouds
			05/22/92	8200–10000	1200	
Tol1924-416	BCG	65.8	11/05/91	3200–3700	1800	
			11/08/92	3700–6900	1200	
			05/19/92	6900–8200	600	clouds
			05/22/92	8200–10000	1200	
1941-543	HII	118.6	11/06/91	3200–3700	1200	
			11/01/91	3700–6400	2100	
			11/05/92	6400–8200	600	
			11/06/92	8200–10000	1200	
NGC7130	Sy2+SB	109.1	11/06/91	3200–3700	1500	
			10/28/91	3700–6400	1800	
			05/19/92	6400–8200	300	clouds
			05/22/92	8200–10000	600	
NGC7496	Sy2+HII	34.2	11/06/91	3200–3700	1200	
			10/28/91	3700–6400	1800	
			05/20/92	6400–8200	600	clouds
			05/21/92	8200–10000	900	clouds
			05/22/92	8200–10000	1200	
NGC7552	SB	37.8	11/06/91	3200–3700	900	
			11/01/91	3700–6400	1200	
			11/06/92	6400–8200	300	
			11/07/92	8200–10000	600	
NGC7282	Sy2+SB	43.9	11/06/91	3200–3700	900	
			10/29/91	3700–6400	1200	
			11/06/92	6400–8200	300	
			11/07/92	8200–10000	600	
NGC7590	Sy2	39.5	11/04/92	3200–6400	3600	
			11/06/92	6400–8200	400	
			11/07/92	8200–10000	600	
NGC7673	HII	84.7	11/02/92	3200–6400	3600	
			11/06/92	6400–8200	500	
			11/07/92	8200–10000	900	
NGC7714	SB	70.5	11/04/92	3200–6400	3600	
			11/08/92	6400–8200	600	
			11/08/92	8200–10000	900	clouds
NGC7793	HII	5.0	06/01/92	3200–3700	1800	
			10/30/91	3700–6900	1620	
			11/06/92	6900–8200	300	
			11/07/92	8200–10000	600	

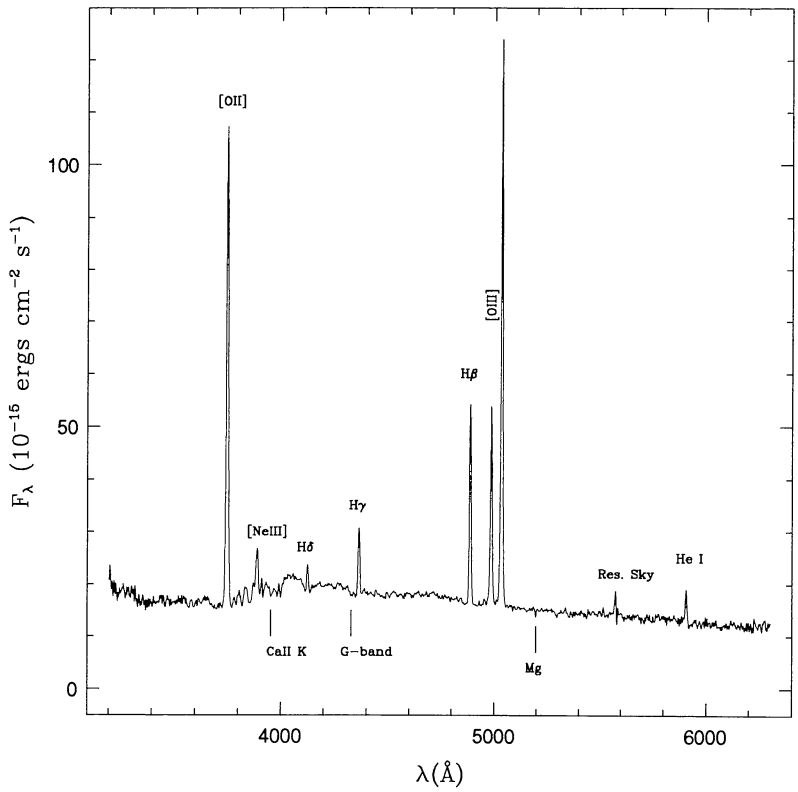

FIG. 1*a*

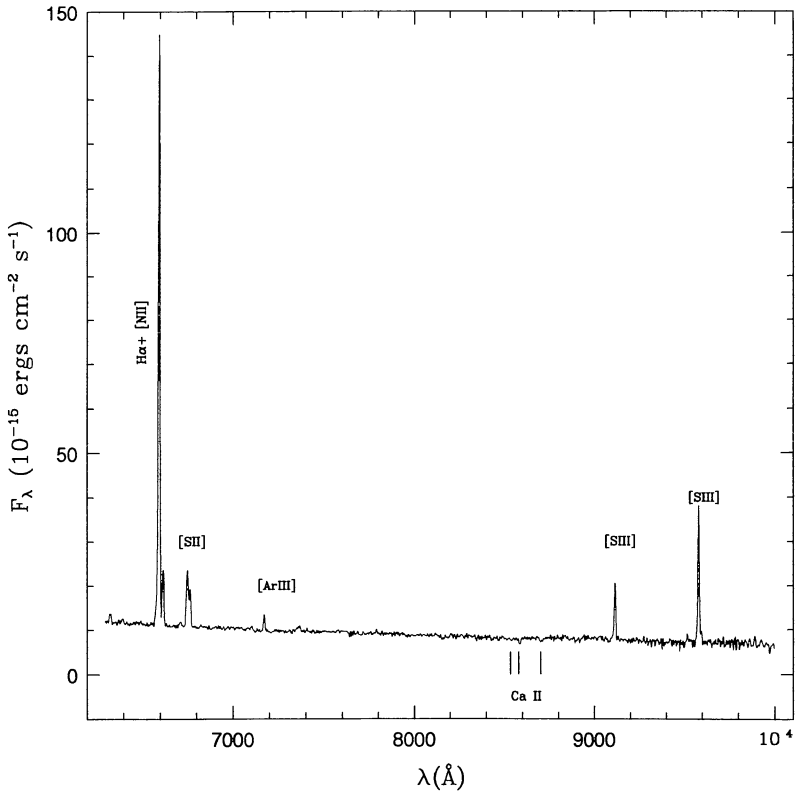

FIG. 1*b*

FIG. 1.—(*a*) Optical and (*b*) near-IR spectrum of the galaxy NGC 1140. The main measured spectral features are identified.

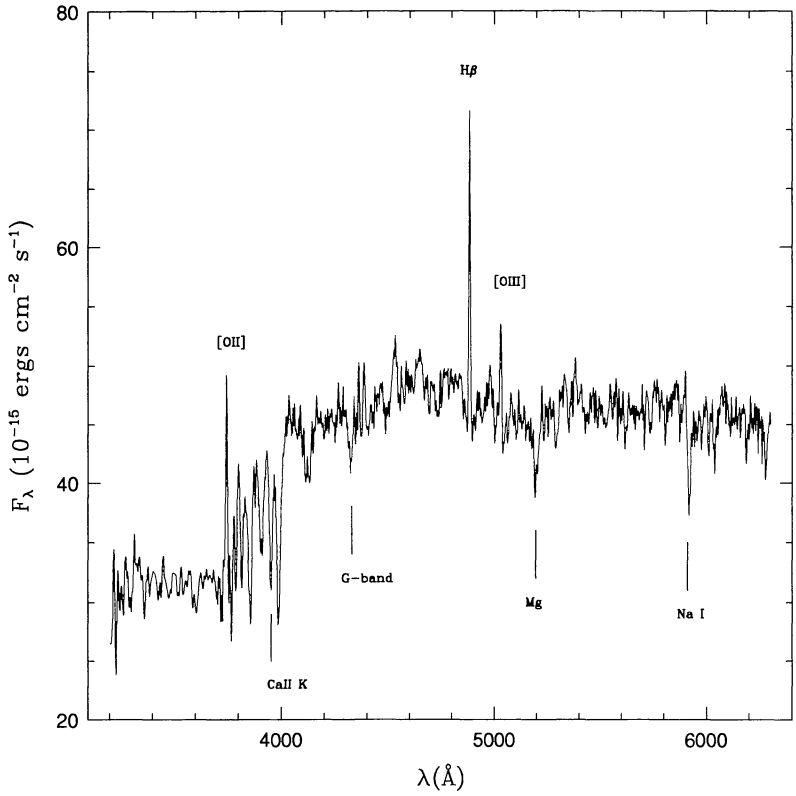

FIG. 2*a*

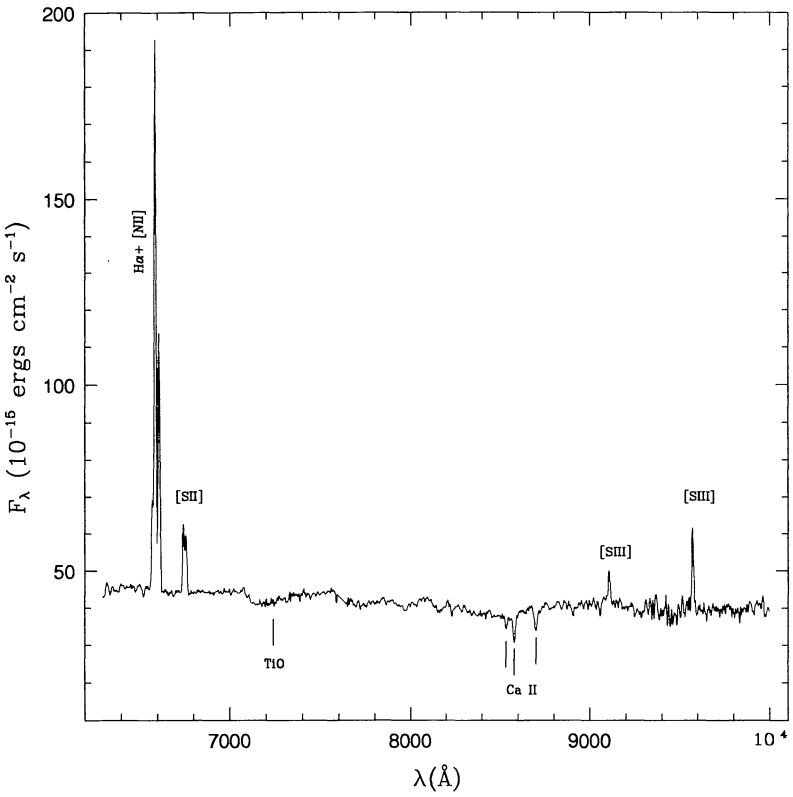

FIG. 2*b*

FIG. 2.—(*a*) Optical and (*b*) near-IR spectrum of the galaxy NGC 1672. The main measured spectral features are identified.

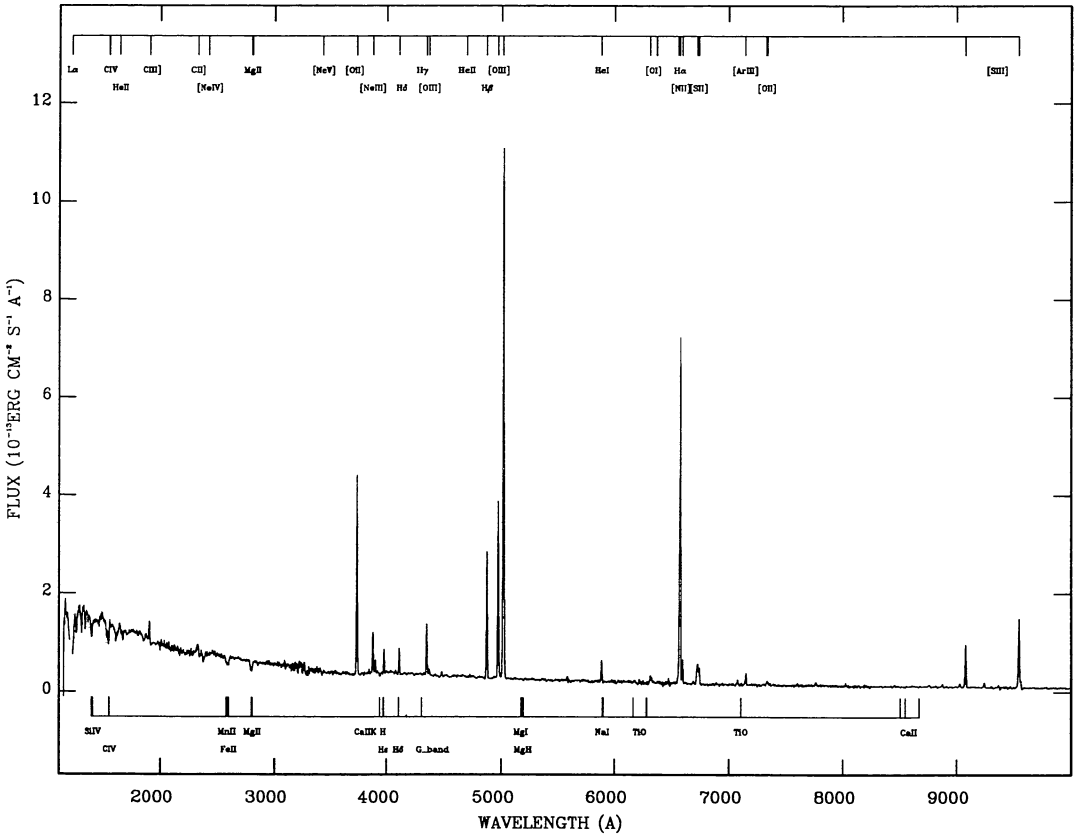

FIG. 3*a*

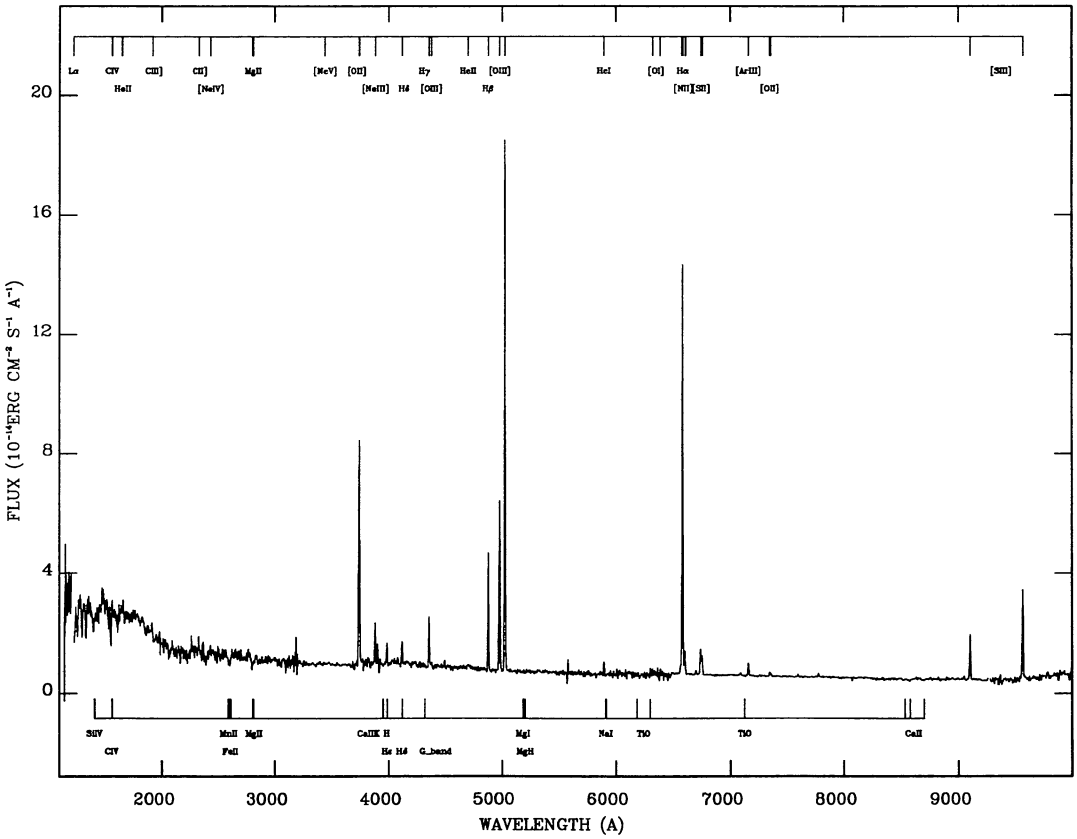

FIG. 3*b*

FIG. 3.—Spectral distributions of three BCGDs. (*a*) NGC 5253, (*b*) NGC 3125, (*c*) NGC 1705.

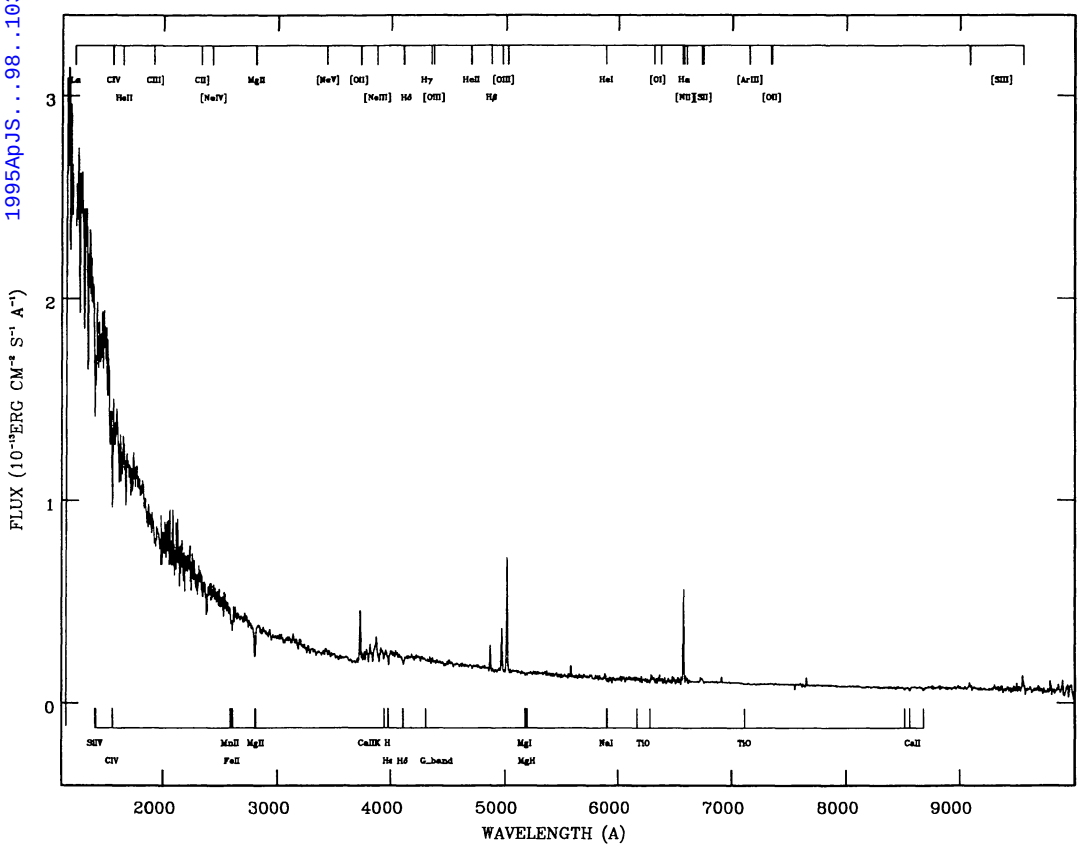

FIG. 3*c*

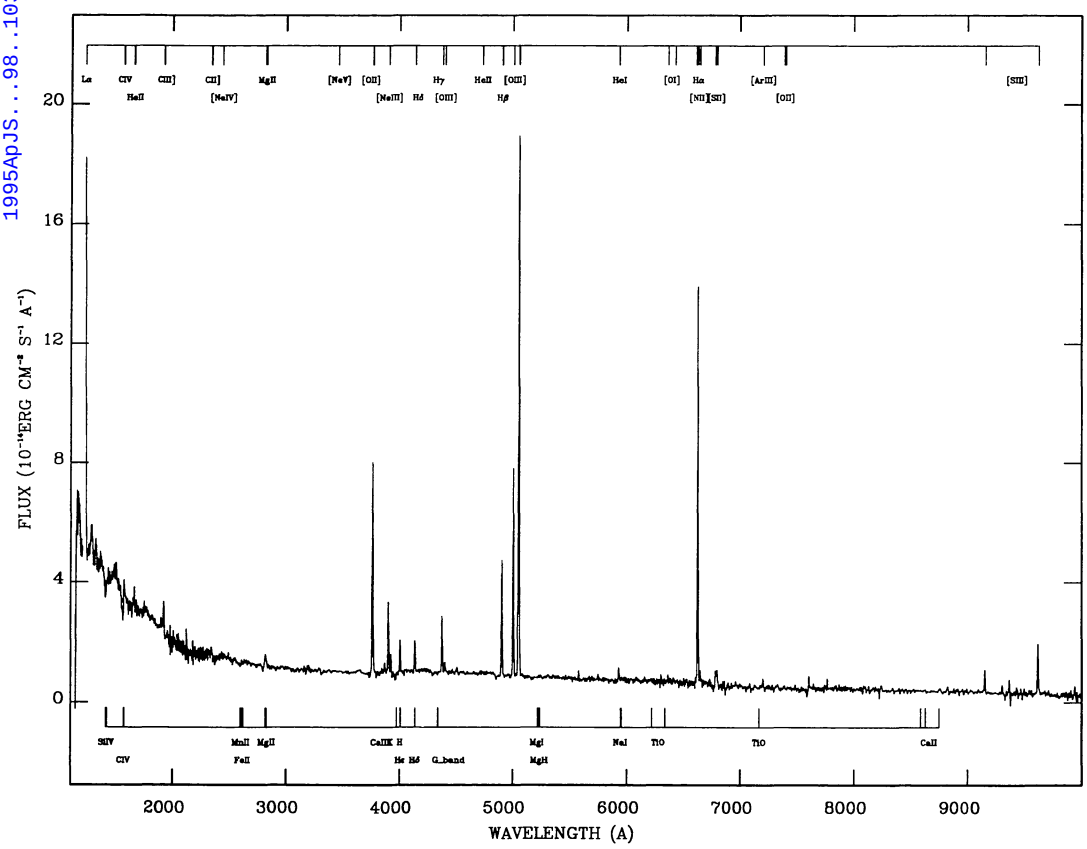

FIG. 4*a*

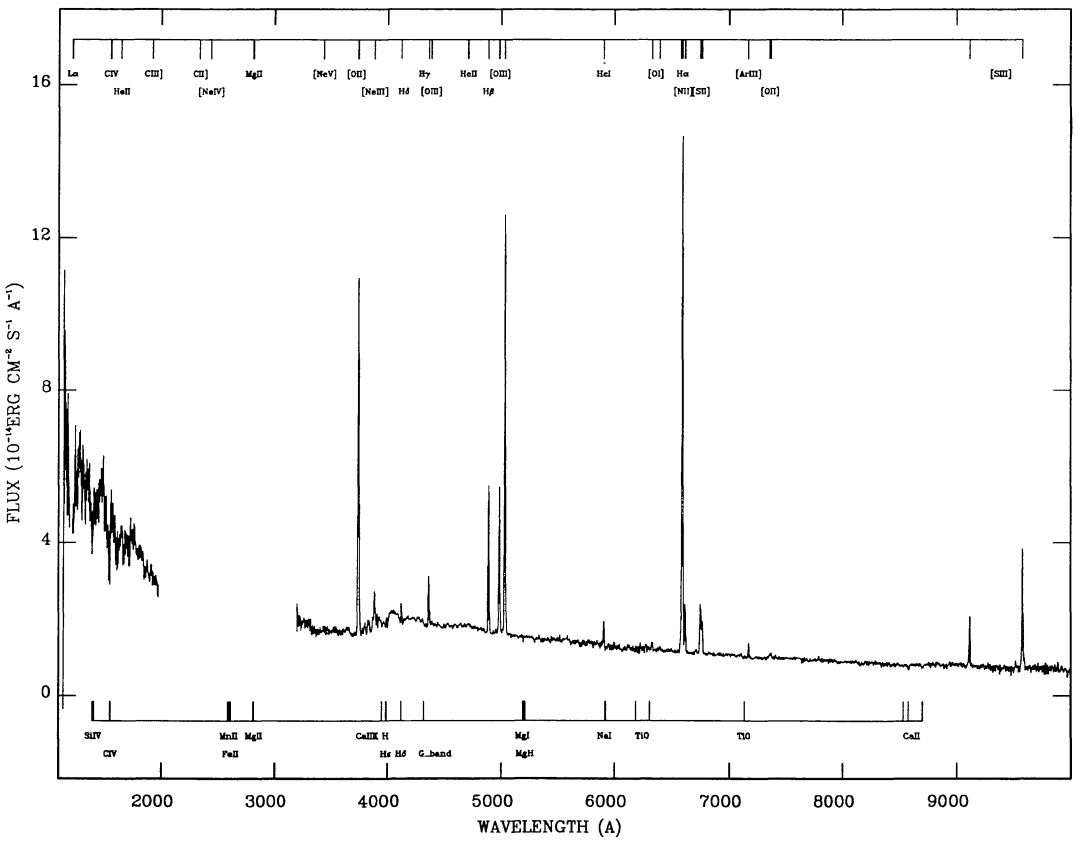

FIG 4*b*

FIG. 4.—Spectra of three BCGs. (*a*) TOL 1924-416, (*b*) NGC 1140, (*c*) 1050 + 04.

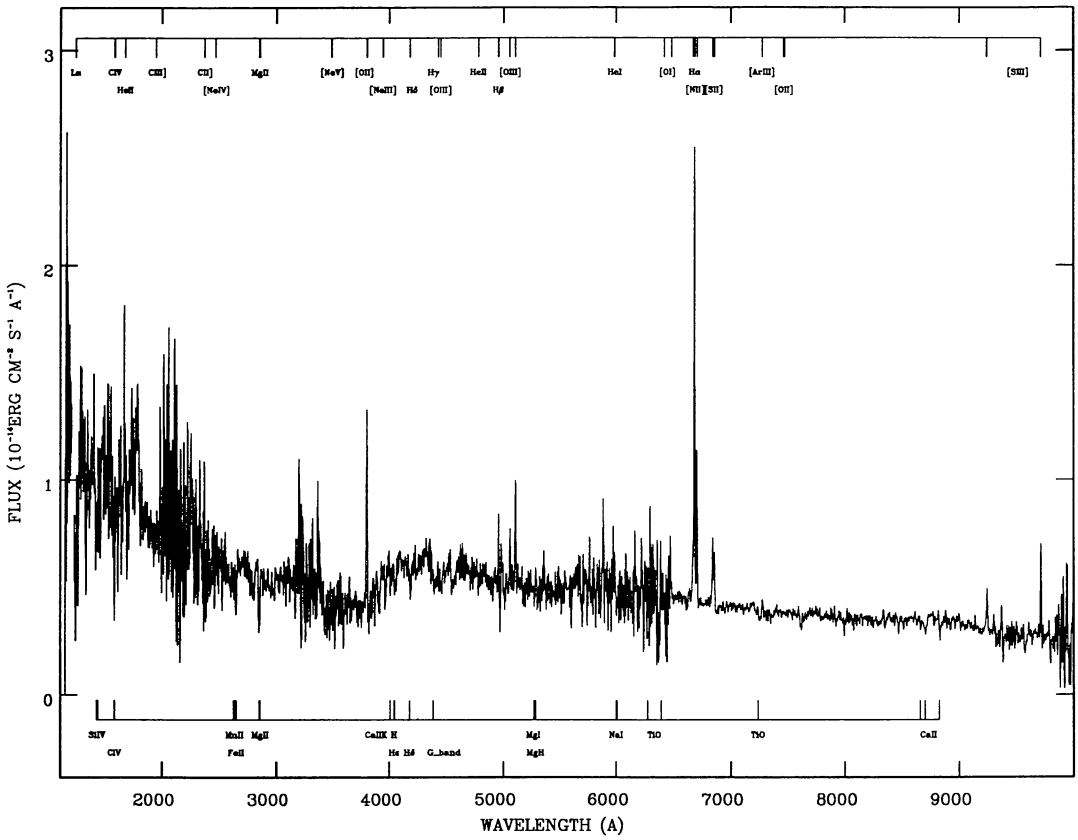

FIG. 4*c*

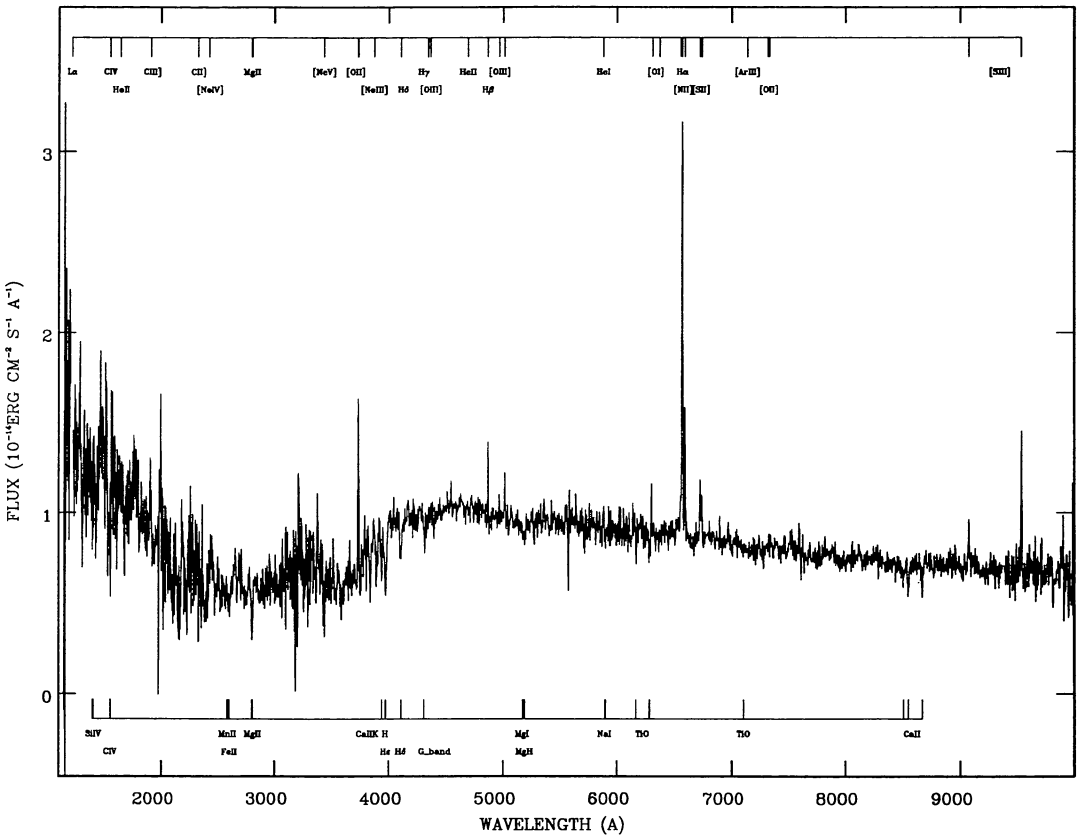

FIG. 5*a*

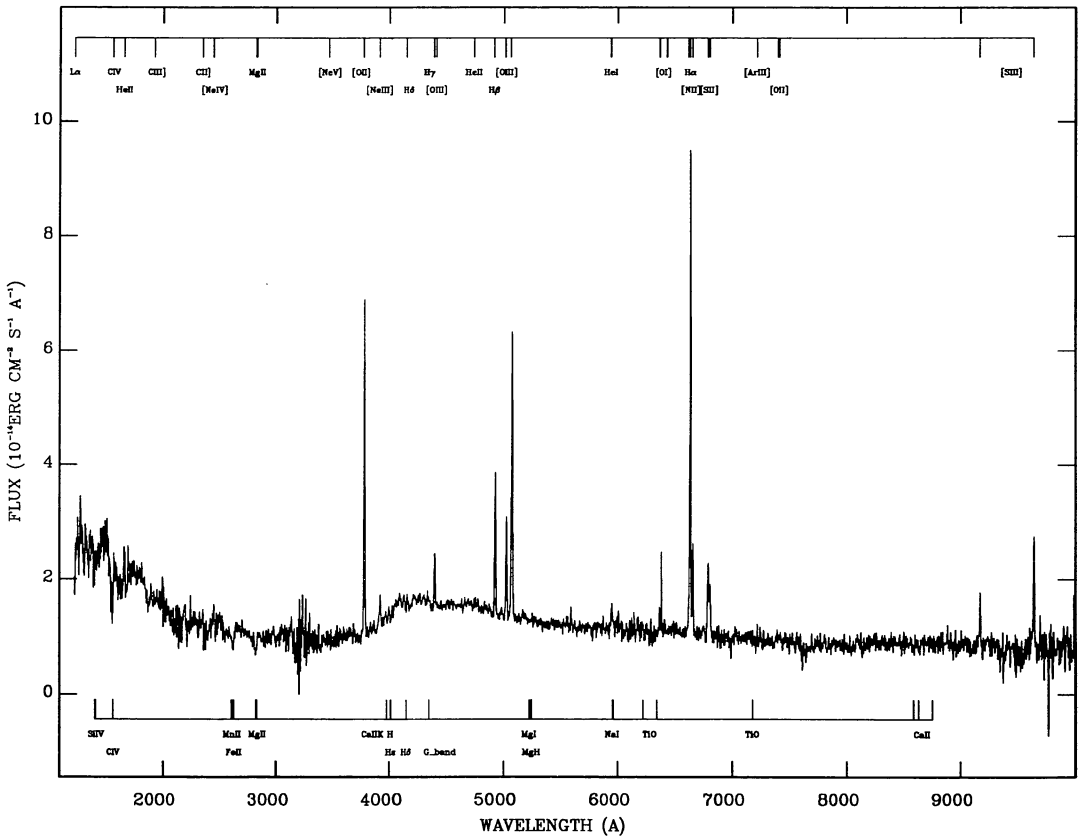

FIG. 5*b*

FIG. 5.—Spectra of two H II galaxies. (*a*) NGC 7793, (*b*) NGC 7673.

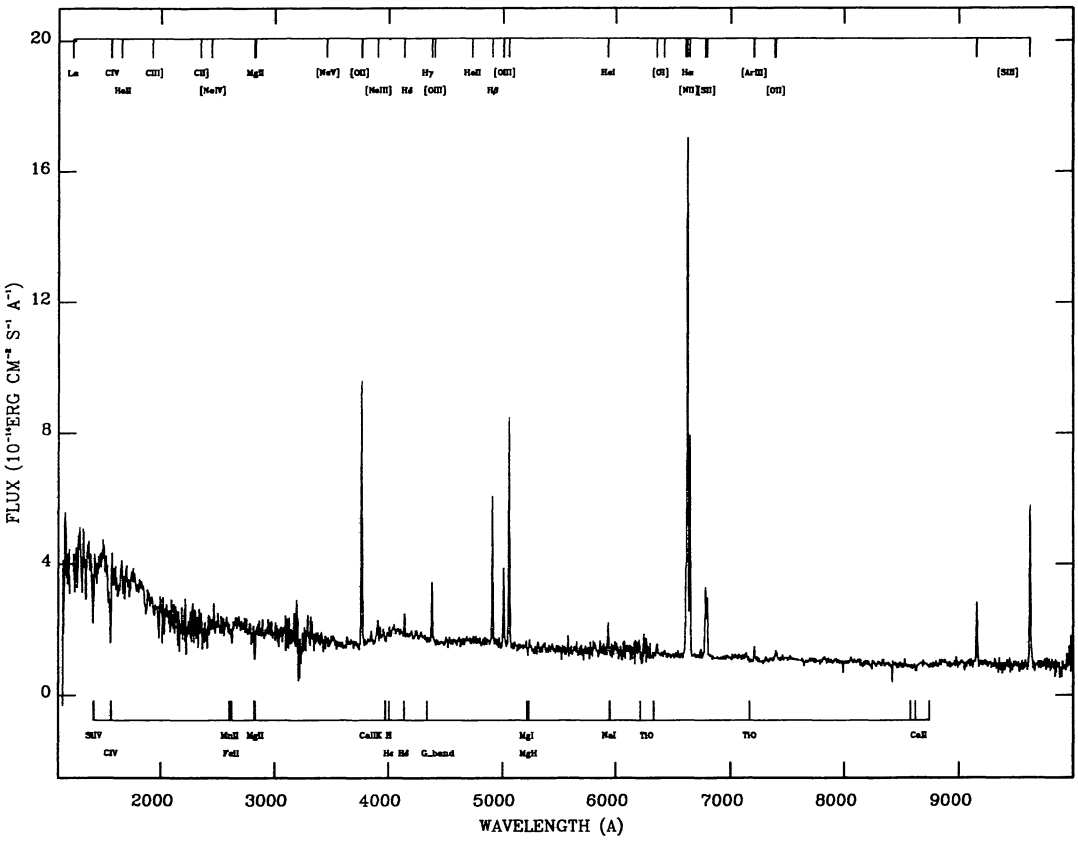

FIG. 6*a*

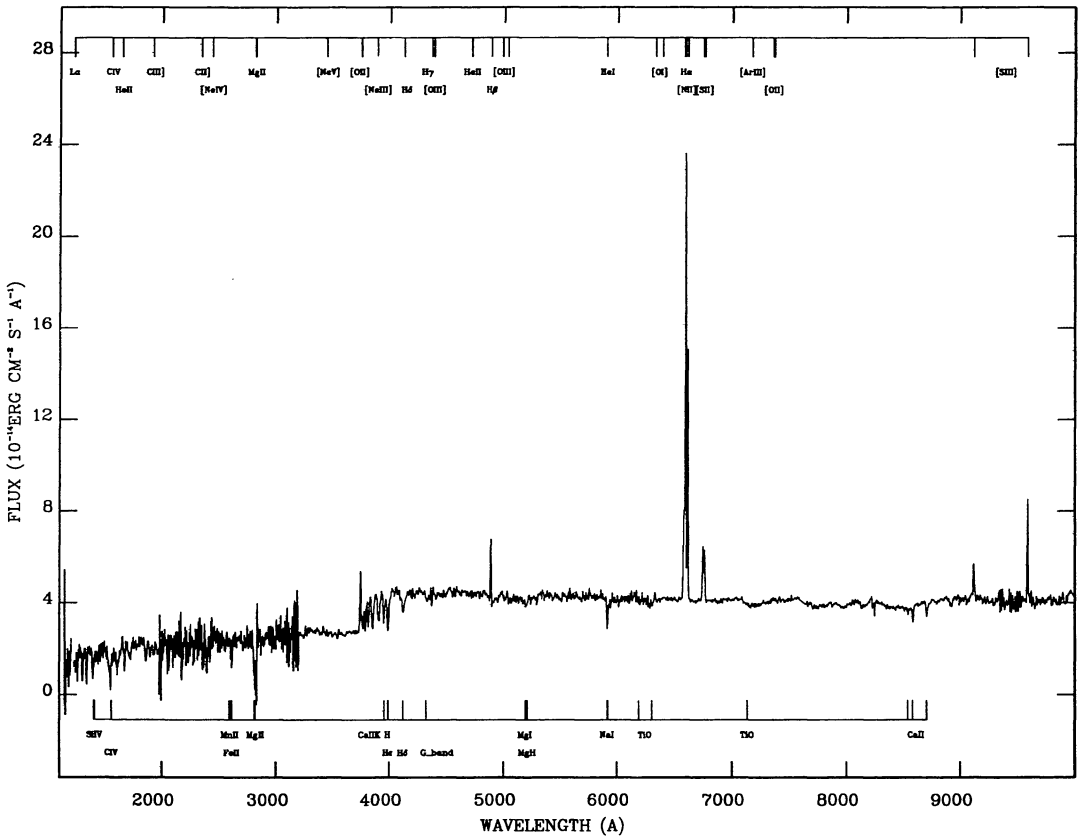

FIG. 6*b*

FIG. 6.—Spectral distributions of three starbursts. (*a*) NGC 7714, (*b*) NGC 7552, (*c*) NGC 5236.

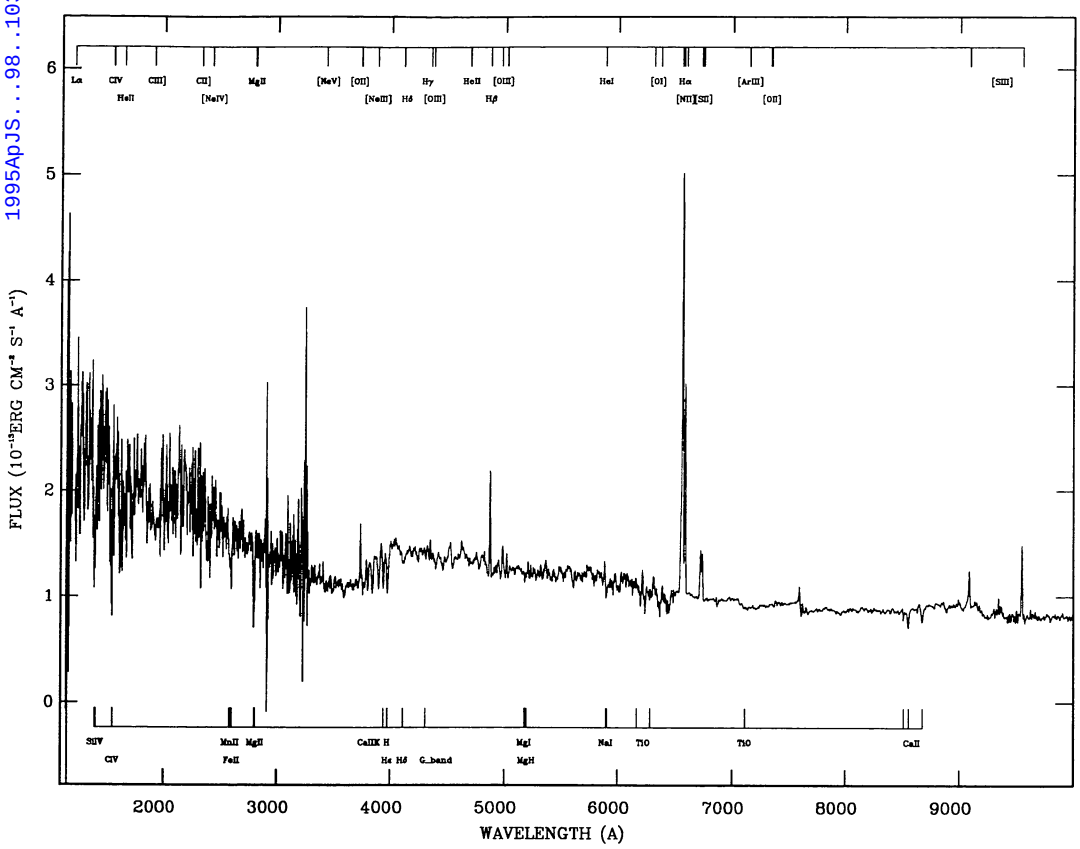

FIG. 6*c*

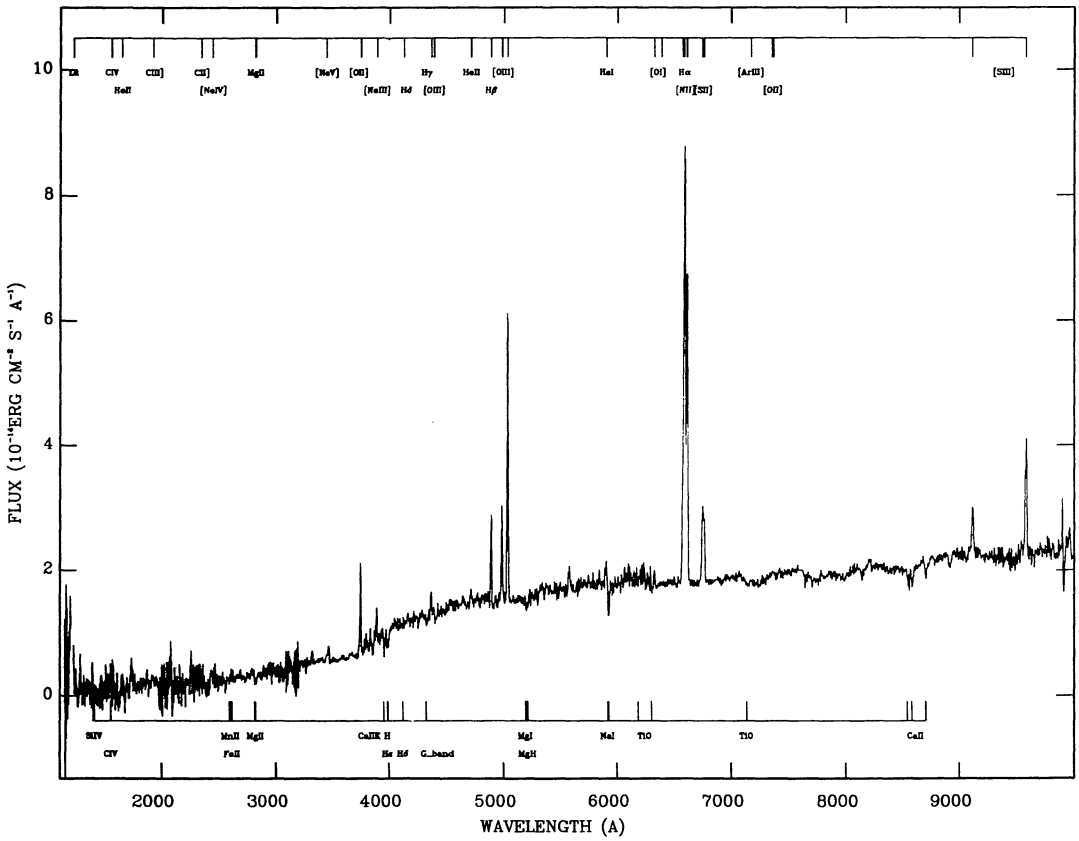

FIG. 7*a*

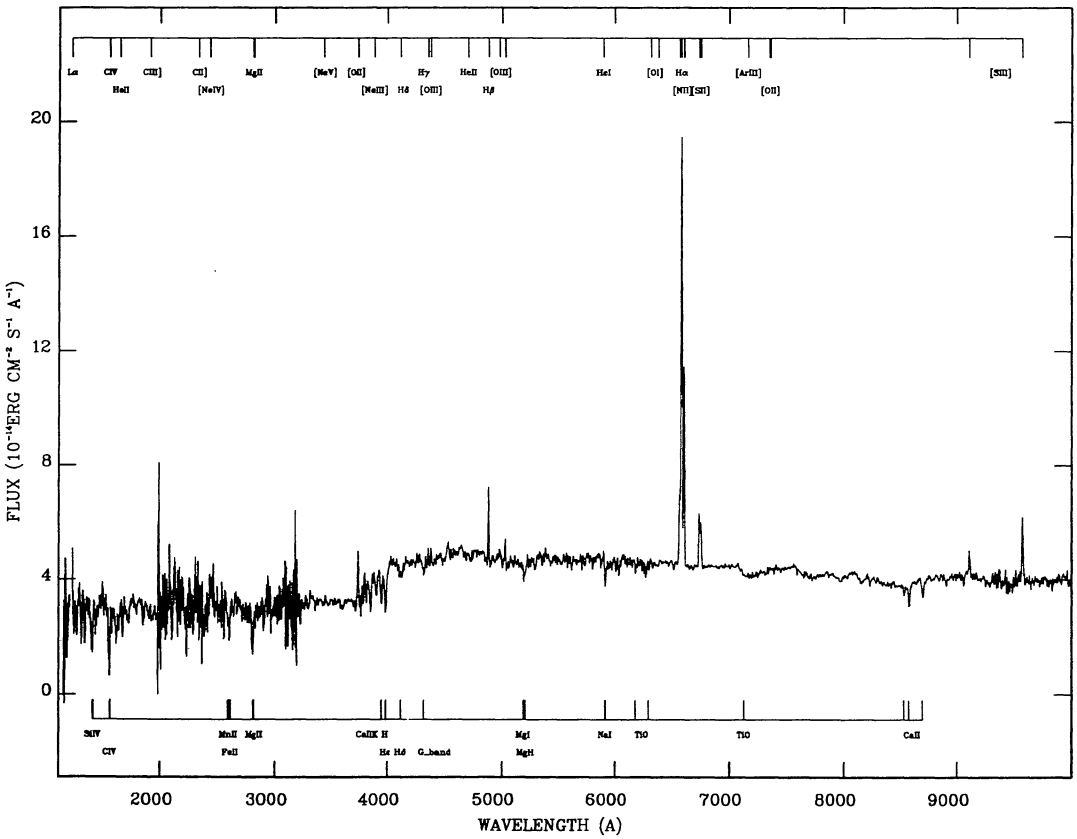

FIG. 7*b*

FIG. 7.—Spectral distributions from two composite-type galaxies. (*a*) NGC 7582, (*b*) NGC 1672.

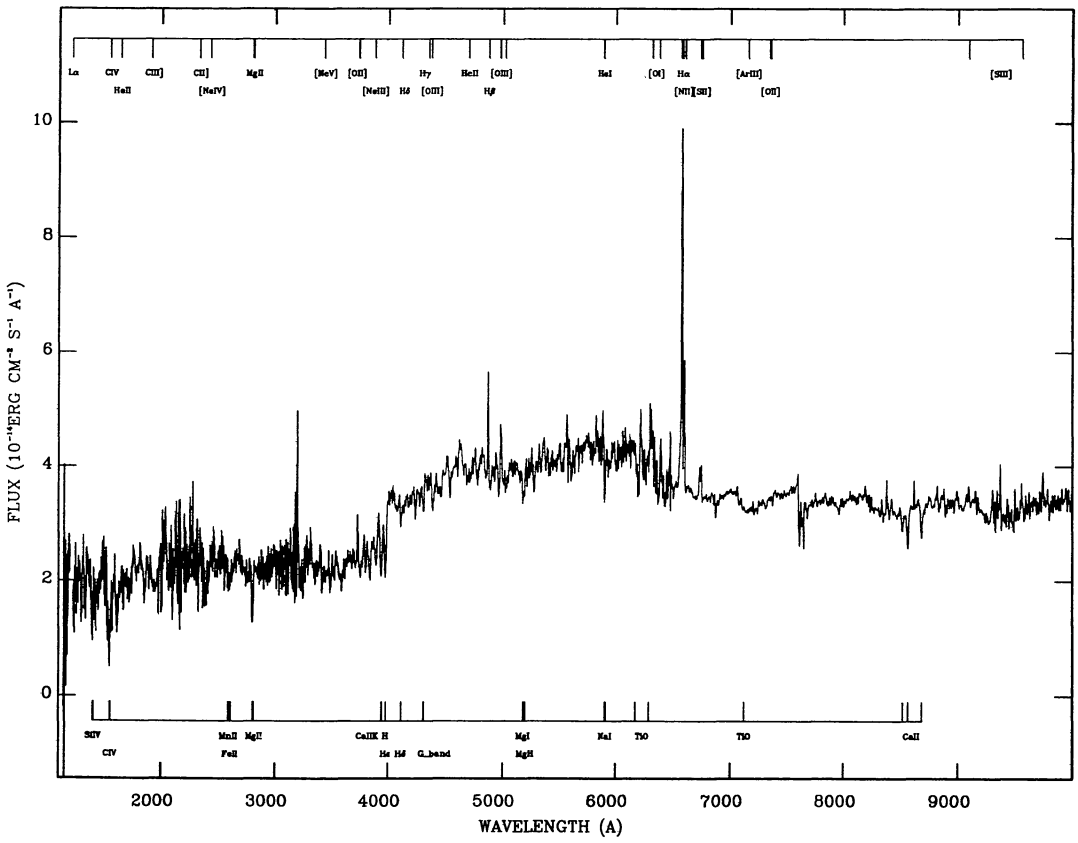

FIG. 8*a*

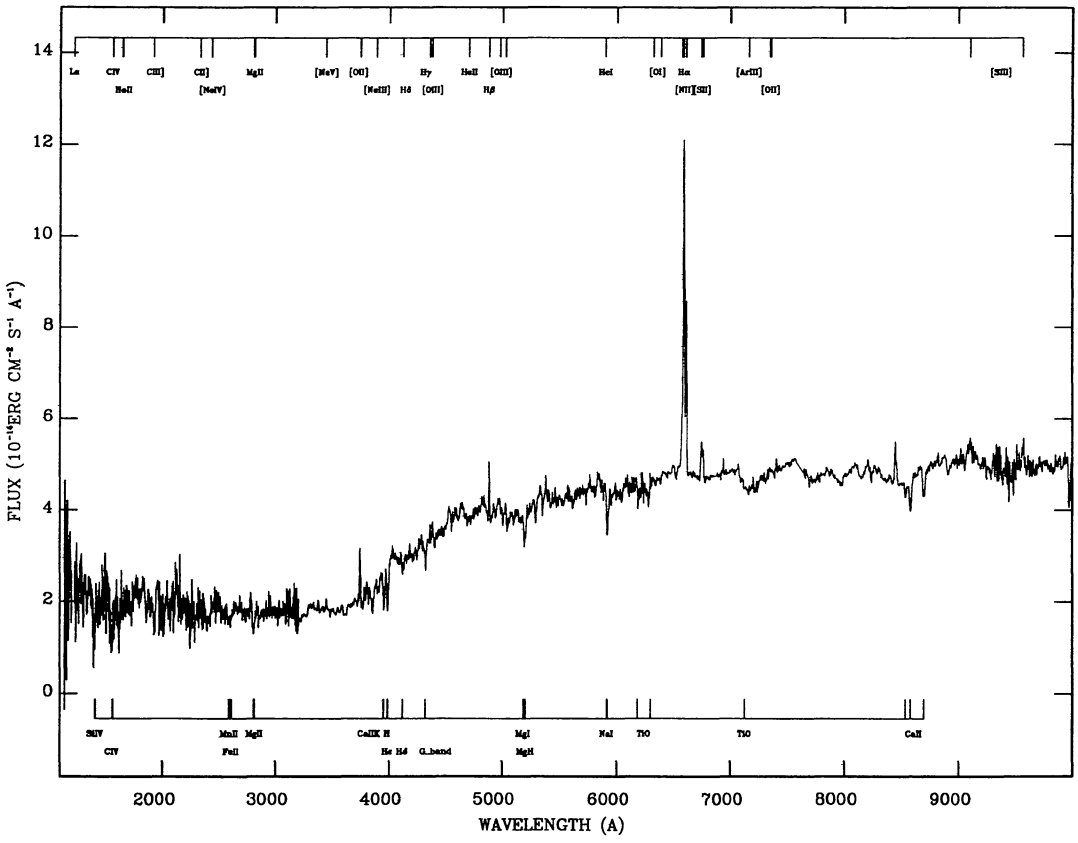

FIG. 8*b*

FIG. 8.—Spectra of the two hot spot galaxies. (*a*) NGC 3351, (*b*) NGC 1097.

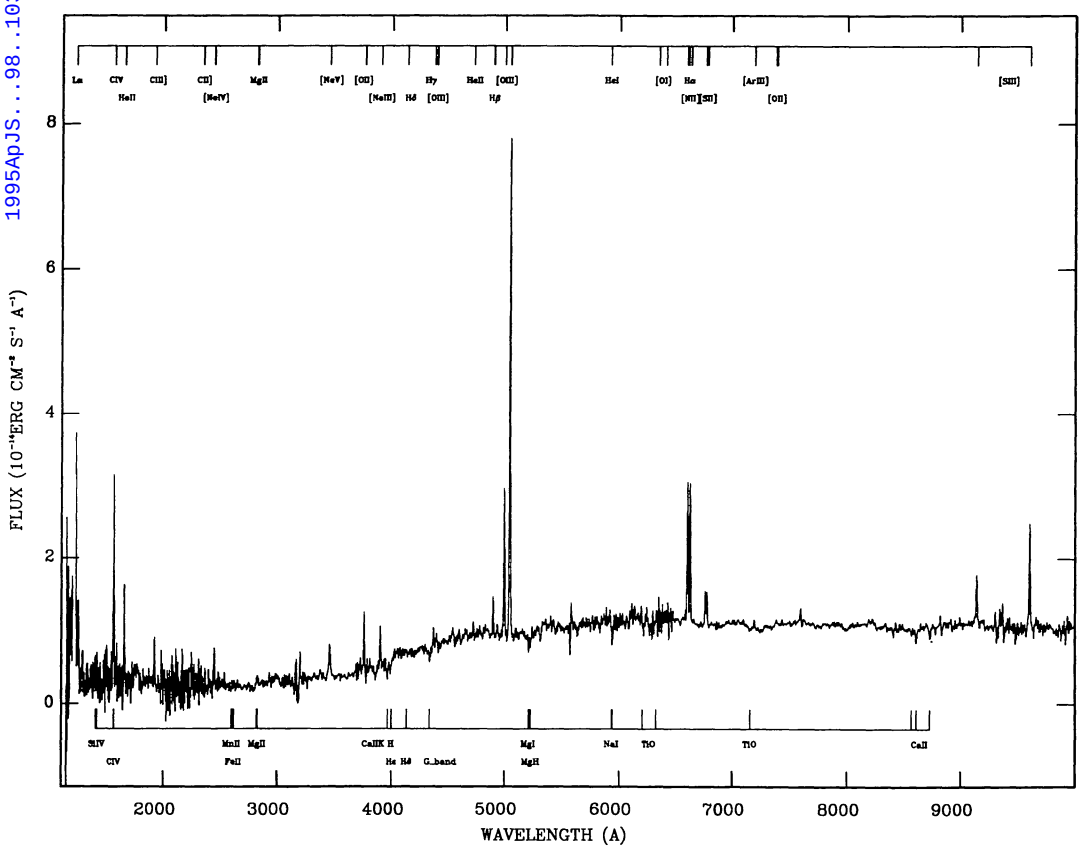

FIG. 9*a*

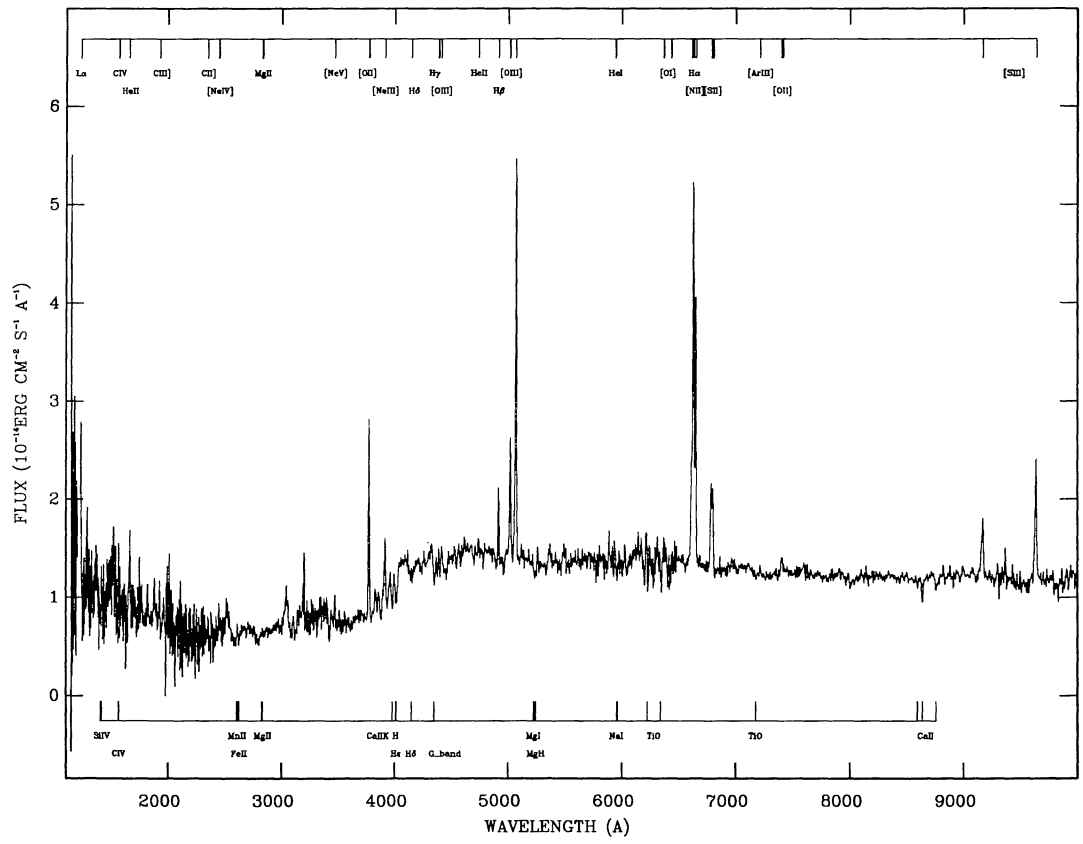

FIG. 9*b*

FIG. 9.—Spectra of two Seyfert 2 galaxies. (*a*) NGC 3081, (*b*) IC 3639.

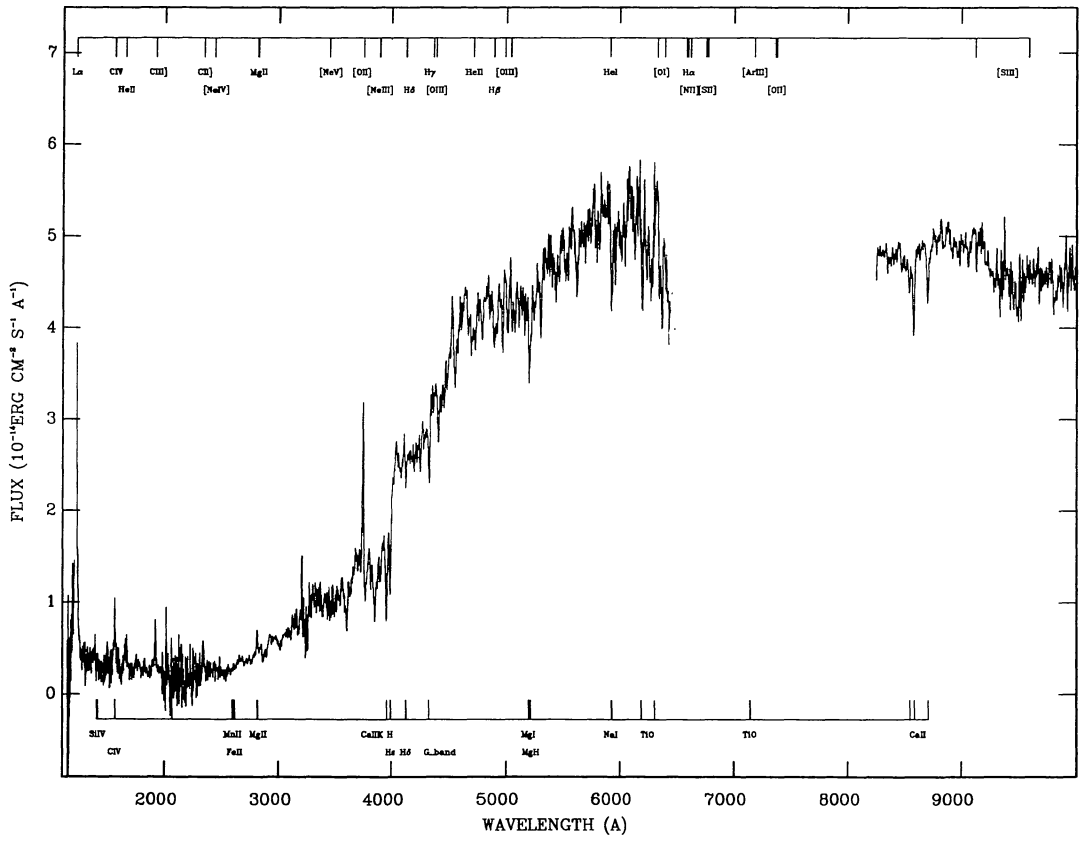

FIG. 10*a*

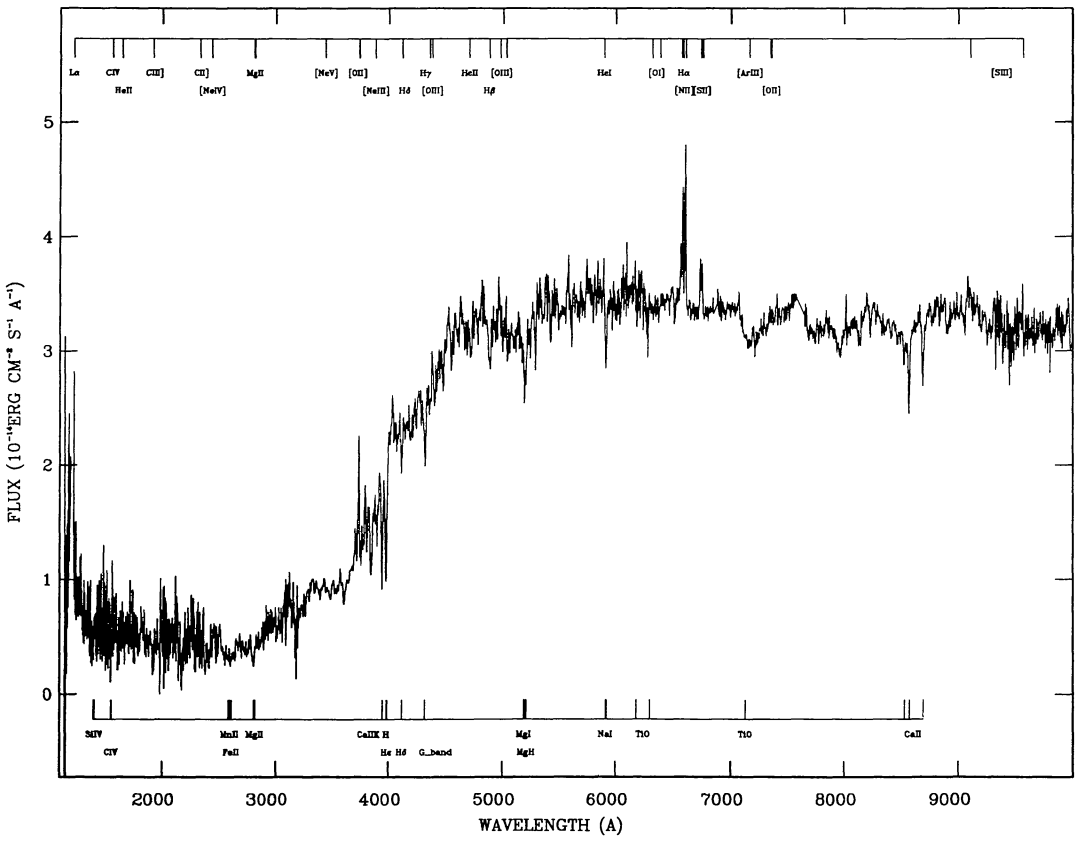

FIG. 10*b*

FIG. 10.—Spectra of two LINER galaxies. (*a*) NGC 4579, (*b*) NGC 1433.

TABLE 2

MEASURED EMISSION LINES

Line Identification	Wavelength (Å)
Lyα	1216
C IV	1548, 1550
He II$_1$	1640
C III]	1908
C II]	2326
[Ne IV]	2424
Mg II	2796, 2803
[Ne V]	3426
[O II]$_1$	3726, 3729
[Ne III]	3869
Hγ	4340
[O III]$_1$	4363
He II$_2$	4686
Hβ	4861
[O III]$_2$	5007
He I	5876
[O I]	6300
[N II]	6584
Hα	6563
[S II]$_1$	6717
[S II]$_2$	6731
[Ar III]	7135
[O II]$_2$	7319, 7330
[S III]$_1$	9069
[S III]$_2$	9532

Figures 1*a* and 2*a* show the range λλ3200–6400 and Figures 1*b* and 2*b* the range λλ6400–10000 for the same galaxies.

The different segments of the spectra were then combined, together with the UV spectra (Kinney et al. 1993), in order to construct spectral distributions from λ1100 to λ10000. The flux levels of the different segments agreeded with each other usually within 10%–20% in the overlapping regions. In a few cases, the differences between the flux levels were larger, mainly when the observations were made under nonphotometric conditions. In these cases, as the UV fluxes should be the most accurate (there is no atmosphere up there in the *IUE!*), before making the measurements, we scaled the optical data to the level indicated by the flux level of the end of the UV spectrum (at $\lambda \approx 3200$ Å). The spectral distributions of the starbursts NGC 7714 (Fig. 6*a*) and NGC 7552 (Fig. 6*b*), of the composite-type galaxy NGC 7582 (Fig. 7*a*) and of the Seyfert 2 NGC 3081 (Fig. 9*a*) are examples for which *no scaling* was necessary between the different segments of the spectra.

3. RESULTS

A sample of the resulting spectral distributions are shown in Figures 3-10. A horizontal bar is drawn at the top of each plot with the location of typical emission lines marked at the redshift of the galaxies. The corresponding rest wavelengths of the lines are shown in Table 2. Beneath the spectrum, another bar shows the location of the main absorption features, whose corresponding windows are listed in Table 3. At least two representative galaxies for each activity class are shown in the figures. We have kept the classification as blue compact dwarf galaxy (BCDG), blue compact galaxy (BCG), HII, starburst (SB), Seyfert (Sy), LINER, composite, and hot spot (Hs) as given by Kinney et al. (1993).

After bringing the spectra to the rest frame, using the radial velocities listed in Table 1 of Kinney et al. (1993), we have measured the fluxes at selected points of the continuum, which have been used in the calculation of equivalent widths of absorption lines and continuum colors. The wavelengths and fluxes are listed in Table 4, together with an estimate of the error for each region of the spectra, calculated as the rms deviation from the average continuum flux at selected wavelengths (the same error estimate can be adopted for neighboring λ's for which the S/N ratio of the spectra do not change significantly). The criteria used in the wavelength selection and determination of the continuum fluxes were the following: for λ1355, λ1455, λ1507, and λ1583, we used averages in the windows, respectively, λλ1348–1365, λλ1435–1475, λλ1500–1515, λλ1565–1600. These were the spectral regions used by Robert, Leitherer, & Heckman (1993) for determining the continuum for the calculation of the equivalent widths of the absorption lines of Si IV λ1400 and C IV λ1550. We decided to this because we have used the results of their work in the analysis of our data. For the region between 2000 and 3500 Å we present the average continuum fluxes in 15 Å bins centered on the wavelengths λ2530 and λ2900, selected because the neighboring spectral regions are free from prominent spectral features. The other continuum wavelengths (in the visual and near-IR) were kindly suggested by E. Bica (see Bica 1988), and most of them sample regions free from emission and absorption lines. The corresponding fluxes were determined as averages in 15 Å bins centered in the listed wavelengths, except for the values corresponding to λ6563 (Hα), which was a visual estimate of the continuum at the base of the line, and λ3810 or λ3780, which were also visual estimates. These last points were necessary for the determination of the continuum in galaxies with strong contribution of late B to F stars which present several high-order Balmer absorption lines in this region. Due to the crowding of the absorption lines, it is difficult to make automatic measurements. We thus selected the higher of the λ3810 and λ3780 fluxes to represent the continuum in this spectral region.

TABLE 3

MEASURED ABSORPTION FEATURES

Window (Å)	Main Absorber	Identification
1380–1415	Si IV	Si IV
1523–1576	C IV	C IV
2570–2615	Fe II	Fe II
2780–2825	Mg II	Mg II
3908–3952	Ca II K	Ca K
3952–3988	Ca II H + Hε	Ca H
4150–4214	CN	CN
4284–4318	*G* band	*G* band
5156–5196	Mg I + MgH	Mg
5880–5914	Na I	Na I
7158–7274	TiO	TiO
8476–8520	Ca II	Ca II (1)
8520–8564	Ca II	Ca II (2)
8640–8700	Ca II	Ca II (3)

TABLE 4

AVERAGE FLUXES AT SELECTED CONTINUUM WAVELENGTHS[1]

galaxy	Wavelengths in Å																			
	1355	1455	1507	1583	2530	2900	3500	3740	3810	4020	4510	4630	5313	5870	6080	6563	7043	7525	8180	8838
HARO15	22.2	22.7	18.9	17.4	—	—	5.3	5.9	7.8	7.4	6.0	5.8	4.5	4.0	3.9	3.4	3.0	2.8	2.5	2.2
			3.0		—	—		0.4					0.3			0.2				0.9
ESO296-11	5.5:	6.5:	6.4:	3.9:	3.2:	3.6:	2.8	2.5	3.2[2]	3.5	3.3	3.2	2.6	2.4	2.2	1.9	1.7	1.6	1.6	1.5
			2.3		1.4			0.3					0.3			0.1				0.3
NGC1068	63.5	60.2	61.1	62.8	45.0	48.9	64.7	71.4	—	100.8	122.0	124.8	138.1	147.1	143.5	135.6	134.4	127.3	134.6	136.5
			2.1		1.6			0.3	—				0.3			5.6				0.3
NGC1097	21.6	20.2	21.1	18.0	17.1	17.7	17.8	20.1	23.8[2]	30.0	39.0	39.5	42.9	45.6	45.6	48.0	48.5	50.1	48.9	50.8
			3.7		1.0			0.6					2.1			0.4				1.2
NGC1140	53.8	51.4	47.1	41.2	—	—	17.0	16.1	19.2	21.5	18.3	18.3	14.8	13.1	12.3	11.3	10.4	9.6	8.7	8.1
			2.1		—	—		0.7					0.5			0.3				0.4
NGC1313	7.4	7.5	8.0	7.1	6.0	5.3	5.0	5.2	6.6[2]	7.6	6.3	6.2	5.0	4.5	4.2	3.8	3.6	3.4	3.1	3.1
			1.0		0.5			0.3					0.2			0.1				0.2
NGC1433	6.7:	6.2:	6.0:	6.1:	4.0	5.8	9.0	12.8	17.2[2]	22.9	31.8	33.6	34.1	34.8	35.1	34.2	33.5	33.9	33.4	33.8
			2.0		0.4			1.3					1.4			0.4				0.9
NGC1510	26.9	25.2	25.1	22.4	9.9	8.7	7.6	8.0	11.1	12.9	10.3	10.2	7.8	7.2	7.1	6.6	6.0	5.5	—	—
			2.1		0.8			0.2					0.3			0.2			—	—
NGC1614	5.8	6.9	4.5	5.5	—	—	5.6	5.7	7.4	8.7	8.5	8.5	8.6	9.4	9.3	9.5	9.8	10.0	10.1	11.1
			1.1		—	—		0.2					0.4			0.2				0.3
NGC1672	30.3	29.5	29.7	26.1	31.3	29.3	31.6	31.7	40.9[2]	45.7	50.5	50.5	47.4	46.2	46.6	44.7	44.4	44.2	41.0	41.4
			1.9		4.1			1.1					1.5			0.5				1.1
NGC1667	3.4	3.3	1.8	2.0	—	—	3.9	4.6	—	8.3	11.3	11.4	11.4	12.6	12.2	12.1	12.2	12.5	12.0	12.6
			1.1		—	—		0.2	—				0.4			0.2				0.5
NGC1705	210.5	175.1	161.2	132.2	47.5	33.8	23.4	22.1	27.7	24.4	19.9	18.7	14.7	12.5	12.0	10.8	10.0	9.1	8.1	7.8
			7.1		2.4			0.6					0.5			0.9				0.4
NGC1800	21.3	15.9	15.1	14.9	—	—	6.8	7.6	9.4	11.5	9.6	9.5	7.9	7.6	7.3	6.6	6.2	5.8	5.1	4.9
			3.2		—	—		0.2					0.2			0.2				0.4
NGC3049	15.3	13.7	14.8	11.8	7.7	6.7	5.3	5.1	5.8	6.5	5.9	6.3	5.2	5.0	5.0	4.1	3.9	3.6	3.4	3.3
			1.4		0.6			0.3					0.2			0.1				0.7
NGC3081	3.0	2.6	2.6	3.1	2.3	3.0	3.7	4.6	—	6.9	9.5	9.5	10.8	11.6	11.7	11.4	11.2	11.1	10.8	11.0
			1.3		0.5			0.7	—				0.5			0.3				0.4
NGC3125	27.9	27.8	27.8	24.5	12.9	11.1	9.6	10.1	10.7	10.7	8.8	8.8	7.3	6.5	6.6	6.5	6.0	5.6	5.1	4.8
			2.7		1.0			0.6					0.3			0.6				0.3
NGC3256	13.2	13.4	13.0	14.0	—	—	13.9	14.2	16.6	18.7	18.0	18.1	17.1	17.1	17.1	15.8	15.6	15.6	15.1	15.8
			1.7		—	—		0.6					0.6			0.5				0.3
NGC3351	21.3	18.8	21.2	17.3	22.8	21.6	22.0	23.2	27.5[2]	35.3	39.6	41.4	40.5	43.2	43.2	36.3	35.0	35.7	34.7	34.3
			3.1		2.1			0.8					1.9			2.8				1.4
NGC3393	1.8	1.7	2.1	1.8	1.4	2.8	3.5	3.8	—	6.1	8.7	9.4	10.5	10.9	11.3	9.9	9.8	9.9	9.3	9.6
			0.8		0.7			0.3	—				0.6			1.1				0.3
1050+04	9.4	9.5	9.1	7.6	5.2	4.8	4.0	3.9	5.2	5.9	5.6	5.4	4.9	4.8	4.6	4.2	3.9	3.7	3.4	3.4
			1.3		0.6			0.4					0.4			0.2				0.2
NGC3660	2.1	2.7	2.6	3.1	1.6	3.6	3.3	3.4	4.4	5.5	7.4	7.5	7.5	7.7	8.1	6.5	6.4	6.3	6.0	6.1
			1.9		0.3			0.4					0.5			0.4				0.4
ESO572-34	27.1	22.7	21.4	18.5	—	—	2.9	2.7	3.0	3.2	2.8	2.8	2.2	2.1	2.0	1.8	1.7	1.6	1.4	1.3
			2.0		—	—		0.3					0.3			0.7				0.4
NGC4385	15.8	16.0	16.5	13.9	9.1	7.8	6.3	5.9	7.7	8.4	8.6	8.7	7.9	8.1	8.8	10.1	9.4	8.7	8.3	8.1
			3.3		0.9			0.6					0.6			0.7				0.5
NGC4569	—	—	—	—	12.6	14.8	16.9	21.4	29.2[2]	41.0	47.2	49.9	49.6	52.2	52.7	—	—	—	43.3	45.6
	—	—	—	—	1.3			0.9					1.9			—	—	—		1.2
NGC4579	4.0	2.4	2.8	3.3	2.3	5.6	10.3	13.6	—	25.8	40.8	42.0	47.2	52.5	53.4	—	—	—	47.8	50.5
			0.8		0.5			0.5	—				1.3			—	—	—		1.0
NGC4594	3.9	5.2	3.4	5.0	2.8	8.9	21.4	30.0	—	55.4	73.9	76.1	92.1	113.2	124.0	122.1	121.7	125.8	122.4	132.6
			2.3		0.5			2.9	—				2.7			2.4				2.5
IC3639	11.3	9.9	11.9	8.0	6.0	6.6	6.8	7.9	10.2[2]	13.0	14.0	14.4	13.9	13.6	14.0	13.2	13.0	12.2	12.0	12.2
			2.7		0.6			0.3					0.6			0.4				0.5
NGC4748	8.6	9.3	10.3	7.6	6.1	5.5	4.5	4.4	—	5.3	6.6	6.9	6.9	7.4	7.4	7.0	6.8	6.8	6.4	6.6
			2.9		0.9			0.3					0.4			0.7				0.3
NGC5102	26.2	24.6	24.5	24.2	18.8	27.1	35.9	42.9	61.4	81.4	79.9	81.4	71.5	69.9	70.7	61.7	58.6	54.8	51.3	50.6
			1.0		1.5			2.2					3.1			1.3				1.3
NGC5135	10.5	10.6	9.2	8.9	10.4	10.9	10.1	10.3	13.5[2]	16.6	17.1	16.9	16.9	17.6	17.3	16.8	16.9	17.1	16.1	17.3
			1.6		2.3			0.6					0.9			0.6				0.6
NGC5236	249.0	245.6	227.8	214.1	162.0	138.0	111.2	117.4	133.2[2]	152.8	143.4	146.0	123.1	118.7	113.3	103.5	97.1	94.1	88.7	93.8
			25.3		9.7			2.6					5.3			6.3				2.6
NGC5253	153.7	143.7	140.0	125.8	72.6	57.8	40.2	36.7	39.8	40.7	33.6	32.7	25.2	23.1	21.8	19.3	16.4	14.2	13.1	11.7
			3.8		2.5			2.1					1.1			3.3				1.6
NGC5506	2.6	1.1	2.6	1.4	1.4	1.5	1.5	2.1	2.7[2]	3.6	4.8	5.1	5.5	6.6	6.6	6.4	6.7	—	6.5	7.2
			2.1		0.8			0.3					0.4			0.7		—		0.8

TABLE 4—*Continued*

	Wavelengths in Å																			
galaxy	1355	1455	1507	1583	2530	2900	3500	3740	3810	4020	4510	4630	5313	5870	6080	6563	7043	7525	8180	8838
NGC5643	0.4	2.3	1.1	1.9	1.6	2.3	4.0	5.2	6.6	9.2	12.0	13.5	14.8	16.8	16.7	17.2	17.1	—	17.2	18.8
			1.8		0.5			0.5					0.6			1.2		—		1.0
NGC5728	3.0	3.2	3.3	2.6	2.1	3.4	4.6	5.5	7.3	10.1	12.8	13.7	14.7	15.6	15.5	14.6	12.4	—	15.6	17.1
			1.4		0.6			0.4					0.8			0.9		—		0.5
NGC6221	2.2:	2.9:	2.3:	1.7:	3.9	4.6	6.1	7.2	8.4[2]	10.9	13.7	14.3	14.3	15.8	16.8	17.9	17.9	18.1	18.5	19.6
			2.5		1.0			0.3					0.6			1.0				0.8
TOL1924-416	43.4	39.2	36.2	31.1	13.4	11.0	9.7	9.1	10.4	10.4	9.6	9.6	8.4	7.4	7.3	6.4	5.4	5.1	4.2	3.7
			1.2		0.6			0.4					0.4			0.7				0.6
1941-543	8.9	9.8	8.0	7.1	—	—	3.7	4.3	4.7	5.0	4.1	3.9	3.1	2.8	2.7	2.1	2.1	1.8	1.7	1.6
			1.8		—	—		0.7					0.4			0.0				0.3
NGC7130	7.3	10.5	7.4	4.9	7.0	7.6	8.2	9.6	12.6	13.5	13.6	13.3	12.9	12.9	12.8	12.4	12.2	11.9	10.5	11.1
			1.5		1.5			0.5					0.4			0.9				0.4
Mrk309	1.7:	2.4:	2.9:	3.3:	—	—	2.8	2.8	2.9	2.9	2.7	2.6	2.4	2.3	2.2	2.1	1.9	1.9	1.9	1.9:
			1.5		—	—		0.2					0.2			0.3				2.7
NGC7496	17.6	14.2	15.5	12.3	9.4	8.7	7.7	8.5	10.2	11.4	10.9	10.9	10.0	9.8	9.6	9.4	9.2	8.8	8.0	8.1
			2.5		0.9			0.4					0.4			0.6				0.5
NGC7552	17.5	18.1	16.9	15.2	22.8	25.0	25.5	30.5	41.4	45.0	44.6	43.6	42.9	42.8	41.9	40.8	41.3	41.5	40.4	41.4
			1.5		1.9			0.4					1.4			0.5				0.9
NGC7582	1.5	0.4	1.6	1.1	2.4	3.9	5.6	7.0	9.8	11.4	14.8	14.9	16.9	17.7	18.6	17.8	18.8	19.9	21.0	22.3
			1.3		0.7			0.3					0.9			0.4				0.7
NGC7590	3.9	3.8	3.4	4.2	3.0	3.3	6.2	6.7	9.3[2]	12.6	14.3	15.2	15.9	17.3	17.5	17.1	17.1	17.5	16.9	17.3
			1.4		0.6			0.6					0.8			0.4				0.6
NGC7673	24.0	24.1	22.0	18.9	10.3	9.5	9.6	10.5	12.1	16.1	15.2	15.3	12.1	11.3	11.0	10.5	9.7	8.9	8.8	8.7
			2.0		0.7			0.8					0.5			0.7				1.2
NGC7714	39.9	38.5	36.5	33.1	20.0	19.0	15.0	15.4	18.4	19.8	15.8	16.5	14.6	13.7	13.7	12.0	11.5	10.6	9.7	9.3
			1.3		1.4			0.6					1.3			0.6				0.6
Mrk542	6.6:	8.2:	7.2:	5.2:	—	—	2.9	2.9	4.0[2]	4.2	4.0	3.9	3.5	3.3	3.3	2.6	—	—	—	—
			1.7		—	—		0.3					0.2			0.5	—	—	—	—
NGC7793	12.8	13.5	13.7	12.2	5.7	5.9	6.1	6.2	9.3	9.9	10.5	10.5	9.6	9.4	9.2	8.5	8.4	8.3	7.5	7.2
			2.9		0.6			0.6					0.6			0.4				0.3

[1] Fluxes in units of 10^{-15} ergs cm^{-2} s^{-1} Å^{-1}. Second line shows the rms deviation from the average continuum value for selected wavelengths (see test).
[2] The listed flux corresponds to λ3780 instead of λ3810.

The above continuum points were then connected by straight lines which were used as the continua for the calculation of equivalent widths (W) of the absorption features listed in Table 3. The results are presented in Table 5. A dash in the table indicates either that the corresponding segment of the spectrum is lacking or that the spectrum was too noisy in the region to give a reliable value for W. Typical errors in the measured W are about 1 Å.

The fluxes of the emission lines (identified in Table 2) have then been measured for the whole sample and are listed in Tables 6 and 7: in Table 6 we present the fluxes of the main emission lines in all the spectra, and in Table 7, we list the fluxes of the emission lines in the UV, He II λ4686, [Ar III] λ7135, and [O II] λλ7319,7330, which can be measured only for a few galaxies. For each galaxy we present, besides the fluxes in the first line of the table, an estimate of the error in the second line. The error was calculated as the product between the rms deviation from the average continuum value adjacent to the emission line and the full width at half-maximum (FWHM) of each line, as we verified that the uncertainties in the continuum are the largest sources of errors in the measured fluxes. These errors are listed only for a few lines, as emission lines with close λ values (e.g. Hβ, [O III] λλ4959,5007) have similar FWHMs and continuum rms, and thus the same errors can be adopted.

4. DISCUSSION

In order to look for general trends in the observed properties, we have grouped the galaxies according to their activity type, and calculated average continuum, emission, and absorption line properties.

4.1. *Emission-Line Properties*

Table 8 shows the average emission-line ratios [O III] λλ4959,5007/Hβ, [N II] λλ6548,6583/Hα, [S II] λλ6717,6731/Hα, [S III] λλ9068, 9532/Hα, and Hα/Hβ. We also show the corresponding standard deviations for each activity type. The ratio [S III] λλ9068,9532/Hα was corrected for reddening, assuming an intrinsic ratio Hα/Hβ = 2.9. The last column lists the number of galaxies in each activity type.

The largest emission-line ratios are presented by the Sy class and are consistent with the predicted ratios for Seyferts galaxies in the diagnostic diagrams for the optical of Baldwin, Phillips, & Terlevich (1981) and for the near-IR of Osterbrock, Tran, & Veilleux (1992). The Hα/Hβ ratio, although among the highest ones, is comparable to that of the SBs, composite and Hs's.

Among the non-Seyfert galaxies, there is a trend in the emission-line ratios from BCDG, through BCG and H II to SBs: [O III]/Hβ decreases while [N II]/Hα increases, which is con-

TABLE 5

EQUIVALENT WIDTHS OF ABSORPTION LINES (Å)

Galaxy	Si IV	C IV	Fe II	Mg II	Ca K	Ca H	CN	Gband	Mg	Na I	TiO	CaII(1)	CaII(2)	CaII(3)
Haro15	8.1	4.4	—	—	4.5	6.6	2.8	2.1	3.2	2.9	—	—	—	—
NGC1097	10.1	11.4	3.2	5.8	7.7	7.4	5.6	5.0	6.6	5.1	8.1	4.8	6.1	4.7
NGC1068	em[1]	em[1]	0.3	em[1]	9.4	1.5	4.2	3.5	3.5	2.0	8.7	3.9	5.5	4.2
NGC1140	5.1	3.9	—	—	3.1	4.1	1.7	1.8	1.2	0.2	4.4	2.9	3.9	2.8
NGC1313	4.3	4.5	7.5	7.4	3.3	6.9	0.4	2.0	2.0	-0.3	4.7	1.5	4.1	3.3
NGC1433	—	—	—	—	11.8	10.6	6.7	6.9	7.0	3.6	8.0	4.5	6.3	5.0
NGC1510	3.7	5.0	3.3	3.0	4.7	6.2	3.4	3.7	1.3	0.1	3.7	—	—	—
NGC1614	—	7.4	—	—	3.4	5.9	1.2	2.4	2.5	4.8	4.6	3.9	4.8	4.5
NGC1672	8.6	11.8	7.3	12.4	6.1	8.1	2.9	3.6	5.0	3.1	6.6	4.9	6.4	5.0
NGC1667	21.2	9.1	—	—	10.1	9.9	7.2	6.9	6.6	3.8	7.7	4.0	5.3	5.3
NGC1705	5.0	6.3	4.3	6.5	2.9	4.5	1.6	1.2	3.3	2.7	5.2	4.0	4.3	4.7
NGC1800	6.9	4.3	—	—	3.9	7.9	2.2	3.1	1.6	0.8	5.2	4.8	—	4.8
NGC3049	7.3	13.3	5.1	5.5	—	—	—	—	—	—	—	—	—	—
NGC3081	em[1]	em[1]	—	em[1]	9.9	6.8	7.2	7.7	8.2	4.8	9.7	4.0	5.6	4.5
NGC3125	5.9	3.6	5.0	5.7	—	—	—	—	—	—	—	3.3	4.6	3.4
NGC3256	9.4	10.6	—	—	1.7	2.8	2.3	0.6	2.9	4.1	4.0	3.5	4.8	3.2
NGC3351	8.6	17.2	4.8	7.0	8.6	8.3	5.0	3.0	4.4	3.2	8.1	4.7	6.3	5.3
NGC3393	em[1]	em[1]	—	em[1]	15.8	1.5	10.7	9.4	8.7	3.8	10.7	3.3	4.9	3.7
1050+04	8.8	8.4	4.5	4.8	2.4	5.1	2.7	4.0	2.8	—	—	1.5	4.1	3.2
NGC3660	—	—	4.2	4.9	13.0	10.5	7.1	7.1	5.5	0.1	7.1	1.7	3.7	3.3
ESO572-34	4.7	6.4	—	—	—	—	—	—	—	—	—	—	—	—
NGC4385	8.3	11.5	6.6	8.7	8.1	5.2	5.0	2.6	1.5	2.5	9.7	3.4	4.5	3.3
NGC4569	—	—	6.1	8.5	7.5	10.2	3.2	3.4	4.5	3.9	—	2.8	4.8	4.3
NGC4579	3.0	em[1]	1.3	em[1]	18.0	12.6	11.1	8.6	7.2	3.8	—	3.3	5.4	4.2
NGC4594	—	—	3.9	23.0	17.8	12.2	11.9	6.9	7.5	5.1	11.3	3.6	5.1	4.3
IC3639	8.6	6.9	3.2	3.5	6.0	6.4	2.6	3.3	4.9	2.4	6.8	2.3	4.4	3.7
NGC4748	em[1]	em[1]	1.7	em[1]	6.9	2.0	5.6	4.1	5.7	1.3	10.5	1.0	3.2	3.7
NGC5102	3.8	2.6	5.5	9.1	6.3	10.7	3.4	2.9	2.4	1.6	3.1	2.2	4.1	3.7
NGC5135	11.6	em[1]	—	—	4.7	6.4	3.3	2.7	2.7	2.6	6.6	3.6	5.0	5.5
NGC5236	11.3	12.3	5.8	5.3	4.3	6.2	3.2	1.5	2.5	2.6	6.6	2.9	4.9	4.3
NGC5253	4.5	4.6	6.5	6.3	3.4	em[1]	1.9	0.6	1.8	em[1]	4.1	—	—	—
NGC5506	—	—	—	—	13.3	5.2	8.4	7.7	4.5	4.5	—	0.5	1.1	0.4
NGC5643	—	em[1]	—	em[1]	10.1	6.5	6.3	6.8	4.3	2.6	—	3.2	4.5	4.2
NGC5728	—	em[1]	—	—	10.4	6.5	5.9	4.7	6.1	3.9	—	2.2	4.4	3.2
NGC6221	—	—	—	—	8.3	6.8	3.8	3.1	5.1	1.6	6.0	3.0	4.6	3.5
TOL1924-416	5.1	2.1	2.6	em[1]	7.4	em[1]	-1.2	1.8	1.9	em[1]	6.3	—	—	—
1941-543	7.5	1.5	—	—	2.5	6.1	4.8	3.0	2.1	1.6	3.8	—	—	—
NGC7130	19.8	21.1	4.7	0.5	3.8	5.7	1.2	2.7	4.7	4.5	8.8	3.1	4.8	5.2
NGC7496	9.4	11.1	3.5	6.6	4.5	6.3	3.5	3.5	3.2	3.2	3.5	3.8	4.8	4.0
NGC7552	10.2	11.5	6.9	—	5.2	8.1	2.4	2.6	3.2	5.6	6.1	4.5	5.5	4.3
NGC7582	—	—	—	9.1	7.6	7.2	3.2	3.8	4.8	4.1	7.8	—	5.9	4.2
NGC7590	—	—	—	10.8	11.7	9.5	5.6	7.7	5.0	4.3	9.2	4.1	5.9	5.0
NGC7673	4.7	7.8	5.3	6.2	—	—	—	—	—	—	—	—	—	—
NGC7714	7.5	8.0	3.5	6.4	4.1	2.4	2.0	—	1.6	0.3	7.5	4.1	4.6	2.6
Mrk542	—	—	—	—	6.0	7.8	2.4	2.4	—	—	—	—	—	—
NGC7793	5.6	9.6	3.3	6.0	6.7	10.0	1.6	3.3	4.0	1.6	5.6	4.1	4.6	3.4

sistent with a decreasing gas excitation and increasing metallicity (McCall, Rybski, & Shields 1985; Pagel & Edmunds 1981). The Hα/Hβ ratio also indicates an increasing reddening. The [S II]/Hα and [S III]/Hα ratios do not show any clear trend, being similar in all types, except perhaps in the BCDG, which show a larger [S III]/[S II] ratio, consistent with its higher excitation. We would like to point out that the galaxy NGC 5253, although classified as SB, has all the emission line ratios, continuum and absorption line W values much more similar to the BCDG type. The fact that it can be considered a dwarf galaxy ($M_B = -18.2$) also favors this classification. We have thus considered NGC 5253 as a BCDG in the calculation of the average properties.

The galaxies classified as composite show [O III]/Hβ and [N II]/Hα values intermediate between SBs and Sy's (as expected), and similar Hα/Hβ to both types. Nevertheless, the [S II]/Hα and [S III]/Hα ratios are smaller than the expected intermediate values. This is probably indicating that the starburst activity is dominating the Seyfert activity in our small sample (4 composite galaxies). The Hs galaxies have emission-line ratios similar to the SBs.

We also show in the seventh column of Table 8 the average Hα luminosity for each activity type, calculated using the distances listed on Table 1 and the reddening calculated as above. It can be seen that, on average, the BCDG are the less luminous and the SB are the more luminous in Hα, although there is a large dispersion within each type. For this reason we also show as a second entry in the seventh column of the table, the range in Hα luminosity for each type. It can be seen that the Sy's and the composites show a similar range to that of the SB's.

Although our sample includes also three LINERs, the spectral distributions in the region $\lambda\lambda$6400–8200 are missing (due to bad weather) for two of them. As the strongest emission lines for the LINERs are [O II] λ3727, [N II] $\lambda\lambda$6584,6548, Hα,

TABLE 6

FLUXES OF MAIN EMISSION LINES[1]

galaxy	[OII]$_1$	[NeIII]	Hγ	[OIII]$_1$	Hβ	[OIII]$_2$	HeI	[OI]	Hα	[NII]	[SII]$_1$	[SII]$_2$	[SIII]$_1$	[SIII]$_2$
HARO15	264.6	—	25.7	—	81.0	187.7	—	—	301.1	49.07	51.7	32.3	—	—
	3.2	—	2.8	—		2.1	—	—	2.5				—	—
ESO296-11	135.1	—	18.1	—	36.4	104.5	—	5:	114.9	21.7	30.6	18.4	11.6	41.3
	3.4	—	1.9	—		2.9	—		1.2					3.2
NGC1068	2196.1	1557.6	352.0:	226:	1049.2	13671.3	—	564.7:	7747.2	13910.4	2773.3[2]	—	2996.8	6618.7
	16.5		92.8			37.9	—		176.64			—		118.7
NGC1097	111.0	—	26.8:	—	101.0	19.4	—	—	886.3	468.6	115.0	86.9	—	—
	2.9	—	6.7	—		5.4	—	—	4.7				—	—
NGC1140	1010.0	86.0	121.3	—	350.3	930.5	47.7	—	1400.0	133.0	163.5	103.5	113.4	273.8
	4.9		3.1	—		2.9		—	3.0					4.4
NGC1313	105.4	—	3.5:	—	17.3	31.0	—	—	148.4	24.8	33.9	24.0	13.7	23.0
	2.6	—	2.5	—		1.4	—	—	0.7					9.5
NGC1433	90.0	—	—	—	—	—	—	—	97.0	149.5	49.9	45.0	—	—
	4.1	—	—	—	—	—	—	—	3.8				—	—
NGC1510	340.9	58.2	31.6	10.1	116.8	577.8	24.5	—	512.1	50.7	49.2	35.3	—	—
	2.1		1.2			1.2		—	1.4				—	—
NGC1614	109.6	—	18.8	—	86.1	82.3	11.0	30.6	923.8	491.5	111.6	112.6	147.9	497.0
	2.2	—	3.7	—		1.8			2.2					6.7
NGC1672	169.2	—	42.0	—	253.1	98.9	—	—	1770.0	805.4	216.0	194.4	93.4	275.4
	8.7	—	8.1	—		6.2	—	—	5.7					19.3
NGC1667	43.9	—	—	—	18.33	63.8	—	—	178.5	123.3	38.8	36.2	—	—
	2.0	—	—	—		1.7	—	—	2.0				—	—
NGC1705	265.0	52.8	22.3	—	130.0	599.9	—	—	434.1	16.7	40.0[2]	—	18.5	49.1
	5.3		5.0	—		3.7	—	—	8.6			—		8.1
NGC1800	199.3	13.0	4.0:	—	26.0	103.8	15.0	—	125.9	21.7	29.9	19.0	15.6	34.4
	2.5		4.8	—		3.2		—	1.7					7.2
NGC3049	148.5	—	51.9	—	116.1	26.3	—	—	513.1	197.7	65.2	55.2	68.8	132.3
	3.9	—	2.8	—		5.7	—	—	1.1					8.6
NGC3081	69.0	50.7	12.0	—	44.5	635.9	—	—	195.8	180.5	42.1	42.0	83.5	166.2
	5.0		3.7	—		5.1	—	—	2.8					4.5
NGC3125	744.9	148.9	149.9	—	368.5	1742.3	54.2	—	1392.0	84.9	101.6	76.0	167.6	326.3
	3.2		4.3	—		5.0		—	6.0					5.2
NGC3256	389.8	—	112.6	—	357.1	167.4	37.6	—	2501.0	1093.2	357.0	290.9	259.1	632.0
	6.3	—	7.5	—		5.5		—	5.8					5.8
NGC3351	58.4	—	—	—	160.9	—	—	—	756.4	279.4	64.0	68.7	—	—
	6.9	—	—	—	13.0	—	—	—	29.5				—	—
NGC3393	291.2	119.1	63.0	23.50	146.0	1603.2	30.0	—	511.9	539.7	155.2	139.2	176.6	397.5
	3.2		6.1			4.8		—	13.9					7.4
1050+04	93.3	—	—	—	26.0	43.5	—	—	205.2	68.9	39.2	26.2	22.2	44.0
	3.2	—	—	—		4.1	—	—	2.0					1.8
NGC3660	—	—	—	—	—	33.7	—	—	55.85	45.7	—	—	—	—
	—	—	—	—	—	2.5	—	—	3.8		—	—	—	—
ESO572-34	283.7	27.8	52.8	—	106.7	419.3	—	—	647.9	45.5	57.6	40.6	46.9	89.1
	3.2		1.7	—		1.5	—	—	8.1					7.4
NGC4385	261.0	—	51.2	—	150.7	119.2	—	—	950.0	466.8	108.2	114.9	185.6	517.9
	4.7	—	3.5	—		5.6	—	—	5.0					4.0
NGC4569	109.2	—	—	—	—	—	—	—	—	—	—	—	23.7:	46.4
	21.1	—	—	—	—	—	—	—	—	—	—	—		9.0
NGC4579	238.7	—	—	—	—	—	—	—	—	—	—	—	—	—
	12.0	—	—	—	—	—	—	—	—	—	—	—	—	—
NGC4594	—	—	—	—	—	—	—	—	—	235.2	—	—	—	—
	—	—	—	—	—	—	—	—	—	29.4	—	—	—	—
IC3639	209.7	59.1	—	—	85.9	456.5	—	—	477.9	330.1	116.1	110.5	110.8	204.3
	3.5		—	—		8.5	—	—	5.1					6.9
NGC4748	61.7	23.1	—	—	57.4	346.8	—	—	334.1	259.8	44.6	50.9	51.6	130.2
	2.8		—	—		2.7	—	—	8.9					4.4
NGC5102	95.0	—	—	—	—	—	—	—	—	45.6	37.9	36.8	—	—
	16.6	—	—	—		—	—	—	15.2					—
NGC5135	168.4	41.5	—	—	87.1	374.7	—	—	693.3	599.9	127.8	110.0	90.6	170.4
	6.8		—	—		5.2	—	—	7.4					8.6
NGC5236	440.0	—	154.7	—	940.1	205.0	—	—	4507.0	2271.8	544.7	495.2	388.7	750.1
	21.0	—	28.8	—		41.6	—	—	66.0					26.5
NGC5253	4370.3	735.5	973.2	84.4	2406.0	11280.2	410.5	96.9	7717.0	565.8	643.8	471.2	970.0	1584.0
	21.6		10.7			10.6			35.0					14.5
NGC5506	174.9	37.7	8.3:	2.4:	56.9	521.4	6.8:	60.6	386.6	354.1	130.8	118.3	138.2	315.2
	2.7		2.3			2.6			7.8					12.1
NGC5643	204.3	47.8	—	—	50.56	788.8	—	63.8:	282.3	351.7	117.4	99.9	123.2	269.5
	3.0		—	—		13.4	—		11.9					13.9

TABLE 6—*Continued*

galaxy	[OII]$_1$	[NeIII]	Hγ	[OIII]$_1$	Hβ	[OIII]$_2$	HeI	[OI]	Hα	[NII]	[SII]$_1$	[SII]$_2$	[SIII]$_1$	[SIII]$_2$
NGC5728	125.3	56.4	—	—	55.5	677.8	—	—	379.1	403.2	57.3	56.7	87.7	223.7
	4.0		—	—		8.2	—	—	9.9					7.2
NGC6221	94.4	—	33.9	—	125.2	71.9	—	—	985.1	642.1	103.5	113.3	135.0	346.7
	3.1	—	5.4	—		9.7	—	—	11.8					12.4
TOL1924-416	686.4	214.7	170.6	27.59	357.9	1744.2	41.8	—	1121.0	26.4	54.0	60.5	66.6	151.1
	4.4		3.5			5.1		—	5.7					5.3
1941-543	205.9	23.5	26.2	—	66.7	244.4	—	6.0	281.0	26.4	32.8	25.7	18.5	46.5
	7.1		3.2	—		2.2	—		0.1					5.7
NGC7130	129.5	38.7	—	—	70.5	340.9	—	—	560.8	417.9	76.3	57.2	38.6	81.7
	4.1		—	—		5.2	—	—	11.3					7.0
Mrk309	—	—	—	—	19.9	6.0:	—	—	111.5	85.4	7.0:	8.0:	—	—
	—	—	—	—		1.9	—	—	3.0				—	—
NGC7496	112.9	—	35.4	—	100.9	66.1	—	—	581.9	279.0	98.5	67.5	27.1	62.1
	3.9	—	5.1	—		4.1	—	—	5.3					6.1
NGC7552	243.8	—	44.5	—	277.8	28.6	—	37.2	2064.0	1183.1	284.6	269.2	186.0	510.2
	3.8	—	9.7	—		9.0	—		5.2					30.6
NGC7582	137.6	50.0	26.9	—	159.5	512.5	33.7:	44.3:	936.7	727.1	178.1	147.7	120.0	305.0
	3.4		5.4	—		5.2			5.2					17.3
NGC7590	80.4	—	—	—	27.1	29.1	—	—	147.7	95.9	45.7	33.9	—	—
	6.6	—	—	—		4.7	—	—	3.8				—	—
NGC7673	664.6	42.7	106.8	—	260.9	555.7	34.7	—	771.6	142.6	133.4	89.8	74.7	184.1
	8.7		6.4	—		6.8		—	6.7					12.7
NGC7714	860.6	56.9	171.8	—	423.1	703.1	90.0	40.9	1878.0	702.6	234.5	193.9	206.8	542.1
	6.1		8.0	—		7.9			6.6					9.9
Mrk542	57.7	—	—	—	26.7	21.0	—	17.9	130.5	32.8	—	—	—	—
	2.2	—	—	—		1.4	—		3.9		—	—	—	—
NGC7793	110.6	—	—	—	33.0	18.1	—	—	221.9	74.65	33.8	25.3	25.3	76.7
	7.3	—	—	—		1.8	—	—	3.7					6.0

[1] Fluxes in units of 10^{-15} cm^{-2} s^{-1}. Second line shows error estimates for selected emission lines (see test).
[2] Sum of the fluxes of [S II] $\lambda\lambda$6716, 6731 emission lines.

[S II] $\lambda\lambda$6717,6731, we are left with only the first emission line, so we have not included them in the discussion about the emission. But we would like to point out that the galaxy NGC 1433, classified as a "normal" by Kinney et al. (1993) for presenting a UV spectrum similar to a normal Sb galaxy, has all the above emission lines, with ratios typical of LINERs, confirming the classification as Seyfert-like by Veron-Cetty & Véron 1986). Although Sersic & Pastoriza (1965) point out the presence of an amorphous nucleus, and Buta (1986) of a nuclear ring or lens of about 20″ diameter, the ring is barely outside our aperture. This galaxy thus seems to be another example of a Hot Spot nucleus with a LINER inside, like NGC 1097, but for which, due to its proximity, we have observed only the LINER nucleus.

4.2. *Continuum Properties*

We show in Table 9 two continuum colors, $C(14\text{-}35)$ and $C(40\text{-}53)$, defined as

$$C(14-35) = -2.5 \log \frac{F_{\lambda 1355}}{F_{\lambda 3500}}$$

$$C(40-53) = -2.5 \log \frac{F_{\lambda 4020}}{F_{\lambda 5313}}.$$

There is a clear sequence in the colors, with the BCDGs being the bluest galaxies, followed by the BCGs, then the H II's, the SBs and the Sy. The composite type presents a redder $C(14\text{-}35)$ color than the Sy (although the standard deviation is very high), indicating that some host galaxies are particularly red (or reddened). The LINERs have the reddest colors, and the Hs show similar values to those of the Sy. These results are in agreement with the average UV slopes found by Kinney et al. (1993). We also show in the last line of the table, the continuum colors of NGC 1433: its $C(40\text{-}54)$ color is similar to those of the LINERs, although its $C(14\text{-}35)$ color is somewhat bluer.

4.3. Absorption Lines

We have calculated the average W values of the absorption features which we concluded were present and best defined in most of the spectra. The results are presented in Table 10. The average W of the UV absorption lines of Si IV and C IV increase from about 5 Å in the BCDG to about 9 Å in the SBs. In the Sy's, these lines are most frequently found in emission, but they reach about 14 Å in the composites and Hs's. The behavior of Fe II and Mg II is less clear: there seems to be a mild gradient in Mg II, which increases from 5.6 Å in the BCDGs to 9.4 Å in the composites, but it should be considered with caution as both Mg II and Fe II can have interstellar contributions from the galaxy itself and also from the Milky Way (Kinney et al. 1993).

In the optical, the W(Ca II K) is about the same ($\approx$ 4 Å) from the BCDG's through the SBs, reaching the largest value (18 Å) for one LINER. This is about the largest value also found in normal galaxies (Bica 1988). In the Sy's, Hs's and composites, W(Ca II K) has an intermediate value, which could be due to a combination of a old red population plus

TABLE 7

FLUXES OF LESS COMMON EMISSION LINES[1]

galaxy	Lyα	CIV	HeII$_1$	CIII]	CII]	[NeIV]	MgII	[NeV]	HeII$_2$	[ArIII]	[OII]$_2$
NGC1068	—	3876.1	1319.7	1839.5	476.2	804.4	588.3	2037.6	388.2	—	—
	—	25.0		27.2			62.0	71.2	37.9	—	—
NGC1140	—	—	—	—	—	—	—	—	—	30.0	—
	—	—	—	—	—	—	—	—	—	3.0	—
NGC1510	—	—	—	—	—	—	47.5:	—	—	15.6	9.2
	—	—	—	—	—	—	39.4	—	—	1.4	
NGC1614	—	—	19.5:	—	—	—	—	—	—	13.5	12.2
	—	—	2.4	—	—	—	—	—	—	2.2	
NGC3081	—	199.3	75.5	55.2	—	40.5	—	44.2	20.9	10.7	—
	—	9.7		3.0	—	7.7	—	7.1	5.1	2.8	—
NGC3125	—	—	—	—	—	—	—	—	—	43.1	21.0
	—	—	—	—	—	—	—	—	—	5.8	
NGC3393	964.1	312.5	190.0	98.7	—	52.8	72.9	58.2	38.2	39.8	—
		6.7		2.7	—		11.5	6.3	4.8	13.9	—
ESO572-34	—	—	—	44.9	—	—	—	—	—	—	—
	—	—	—	5.6	—	—	—	—	—	—	—
NGC4385	—	—	—	—	36.3	—	—	—	—	—	—
	—	—	—	—	10.8	—	—	—	—	—	—
NGC4579	—	77.7	—	53.6	—	—	24.8	—	—	—	—
	—	6.9	—	4.7	—	—	1.1	—	—	—	—
IC3639	—	—	—	—	—	—	—	39.4	—	—	23.0
	—	—	—	—	—	—	—	9.7	—	—	5.1
NGC4748	431.2	242.8	88.7	112.8:	—	—	104:	18.8:	—	—	—
		39.9		29.6	—	—	9.8	3.3	—	—	—
NGC5135	509.6	80.8	85.7	—	—	—	—	24.8	—	—	—
		11.5		—	—	—	—	7.7	—	—	—
NGC5253	—	—	—	398.9	—	—	—	—	—	263.0	122.2
	—	—	—	32.7	—	—	—	—	—	35.0	
NGC5506	—	—	—	59.3:	—	—	—	6.4	7.4:	—	—
	—	—	—	11.6	—	—	—	2.4	2.6	—	—
NGC5643	—	85.7	—	42.1	—	—	22.7:	62.4	20.1	—	—
	—	13.2	—	7.3	—	—	4.8	11.7	13.4	—	—
NGC5728	—	89.6	—	—	—	—	—	—	—	—	—
	—	12.1	—	—	—	—	—	—	—	—	—
TOL1924-416	1131.0	—	—	85.7	—	—	73.0	—	—	28.5	—
		—	—	2.4	—	—	5.9	—	—	5.7	—
1941-543	73.8	—	—	—	—	—	—	—	—	—	—
		—	—	—	—	—	—	—	—	—	—
NGC7130	202.0	—	—	—	—	—	—	—	—	—	—
		—	—	—	—	—	—	—	—	—	—
NGC7582	—	—	—	—	—	—	—	—	13.4:	—	—
	—	—	—	—	—	—	—	—	5.2	—	—
NGC7714	—	—	—	—	—	—	—	—	—	32.5	—
	—	—	—	—	—	—	—	—	—	6.6	—

[1] Fluxes in units 10^{-15} ergs cm^{-2} s^{-1}. Second line shows error estimates for selected emission lines (see text).

TABLE 8

AVERAGE EMISSION-LINE RATIOS PER ACTIVITY TYPE

Activity Type	N	[O III]/Hβ	[N II]/Hα	[S II]/Hα	[S III]/Hα	Hα/Hβ	L(Hα)[a]
BCDG	4	6.7 ± 0.6	0.09 ± 0.03	0.13 ± 0.03	0.23 ± 0.09	3.9 ± 0.4	5.3 ± 3.2
							1.0–9.9
BCG	4	3.8 ± 1.6	0.20 ± 0.15	0.22 ± 0.08	0.17 ± 0.03	4.7 ± 1.9	142.3 ± 110.0
							64.4–332.2
H II	6	3.6 ± 1.7	0.22 ± 0.11	0.28 ± 0.09	0.19 ± 0.08	5.6 ± 1.8	28.4 ± 38.1
							0.4–105.9
SB	8	0.8 ± 0.7	0.66 ± 0.15	0.23 ± 0.04	0.22 ± 0.08	6.2 ± 2.0	631 ± 789.4
							11.36–2264.0
Sy	12	11.5 ± 6.2	1.24 ± 0.40	0.47 ± 0.14	0.53 ± 0.25	6.3 ± 1.6	256 ± 344.2
							10.8–1155.0
Composite	5	2.6 ± 2.4	0.81 ± 0.17	0.27 ± 0.05	0.13 ± 0.06	6.9 ± 0.9	228.6 ± 243.2
							36.0–706.9
Hs	2	0.26[b]	0.59 ± 0.10	0.21 ± 0.03	...	6.7 ± 2.0	59.7 ± 52.1
							7.6–111.7

[a] In units of 10^{40} ergs s^{-1}.
[b] Only one measurement.

TABLE 9

AVERAGE CONTINUUM COLORS PER ACTIVITY TYPE

Activity Type	C(14-35)	C(40-53)
BCDG	-1.59 ± 0.47	-0.51 ± 0.05
BCG	-1.34 ± 0.28	-0.35 ± 0.14
H II	-1.14 ± 0.63	-0.36 ± 0.16
SB	-0.31 ± 0.66	-0.15 ± 0.10
Sy	0.06 ± 0.47	0.34 ± 0.16
LINER	1.43 ± 0.41[a]	0.48 ± 0.19[b]
Composite	0.36 ± 0.82	0.14 ± 0.20
Hs	-0.09 ± 0.12	0.27 ± 0.12
N1433	0.32	0.43

[a] Average of only two measurements.
[b] Average of only three measurements.

young blue stars in Hs's and composites or a blue featureless continuum in the Sy's (Kinney et al. 1991; Schmitt, Storchi-Bergmann, & Baldwin 1994). The other optical absorption features: G band, Mg I and Na I, which originate mainly in the red star population, have very small W in the BCDGs, BCGs, H II's, and SBs, indicating the dominance of blue stars in the integrated continuum in these types. For the Sy's, the average values are as large as the one for the LINERs, indicating that the dominant stellar population is old (Storchi-Bergmann, Bica, & Pastoriza 1990) and that the dilution by a blue featureless continuum is smaller (if any) at wavelengths larger that ≈ 4000 Å.

In the last column of Table 10, we show W(Ca II λ8662). We have observed that the Ca II triplet in the BCDGs, BCGs, and H II's was either present with average W(Ca II λ8662) $\approx$ 3–4 Å or not present at all. In the SBs the lines are always present, with average W about the same. In stars, the W of Ca II triplet correlates strongly with surface gravity, being much larger in giants and supergiants than in dwarfs (Jones, Alloin, & Jones 1984). The Ca II triplet in the spectra is thus indicating the presence of giants and supergiants, which are always present in the SBs but not always is the BCDGs, BCGs and H II's, probably due to their absence at early ages of the burst. For the Sy's and composites, W(Ca II) is somewhat larger, and the largest values (5.0 Å) are the ones from the Hs's and NGC 1433. Bica & Alloin (1987) have shown that W(Ca II) is sensitive to metallicity if a whole range $-2.0 < Z/Z_\odot < 0.0$ is considered. Nevertheless, there is a lot of scatter and a smaller correlation if only the range $-1.0 < Z/Z_\odot < 0.0$ is considered, which is our case (Storchi-Bergmann et al. 1994).

4.4. *Discussion of Individual Spectra*

A common characteristic to all the spectra with active star formation (BCG, BCDG, H II, starbursts, composite, and hot spot galaxies) is the presence in the UV of the absorption features of young blue O, B stars (e.g., Si IV λ1400, C IV λ1550) from the present burst of star formation. In the optical range, there is a varying strength of the absorption features, which denote the relative importance of previous bursts of star formation. A general trend (with a few exceptions) is: the higher the abundance (as can be hinted from the [N II]/Hα ratio), more conspicuous are the absorption features from previous generations of stars. The emission-line spectra vary from high excitation (high [O III]/Hβ ratio) for the lower abundance galaxies (BCG, BCDG) to a decreasing excitation as the abundances get higher for the starbursts and hot spot galaxies. We now briefly discuss the different kinds of spectra we obtained for each activity class.

Figure 3 shows the spectral distributions for three BCDGs. NGC 5253 presents very similar spectrum to NGC 3125, confirming our classification of this galaxy as a BCDG. Notice the high [O III]/Hβ and small [N II]/Hα ratio and the almost absence of absorption lines in the optical spectrum. NGC 1705 differs from the two previous ones in presenting relatively strong absorption features in the optical and near-IR due to the presence of an older burst of star formation (Meurer et al. 1992). It is one of the bluest galaxies of the sample.

Figure 4 shows three examples of spectra of BCD galaxies. Tol1 924-416 shows a very similar spectrum to the previous BCDG, the only difference being that it is a more luminous galaxy. NGC 1140 and 1050 + 04 show a lower excitation and higher abundance as indicated by the higher [N II]/Hα.

Two spectra of H II galaxies are shown in Figure 5: NGC 7793 presents a low excitation spectrum with higher abun-

TABLE 10

AVERAGE EQUIVALENT WIDTHS PER ACTIVITY TYPE

Activity Type	Si IV	C IV	Fe II	Mg II	Ca K	G Band	Mg	Na I	Ca II (3)
BCDG	4.8 ± 0.8	4.8 ± 0.9	5.1 ± 1.2	5.6 ± 1.6	3.7 ± 08	1.8 ± 1.3	2.1 ± 0.8	1.4 ± 1.3[b]	4.1 ± 0.7[b]
BCG	6.8 ± 1.7	4.7 ± 2.3	3.6 ± 1.0[b]	4.8[a]	4.4 ± 1.9	2.4 ± 0.9	2.3 ± 0.8	1.6 ± 1.4[b]	3.0 ± 0.2[b]
H II	5.6 ± 1.2	5.7 ± 2.6	5.4 ± 1.7[c]	6.5 ± 0.6[c]	4.1 ± 1.6	2.9 ± 0.5	2.4 ± 0.9	0.9 ± 0.8	3.8 ± 0.7[c]
Sb	8.8 ± 2.5	9.7 ± 3.3	5.6 ± 1.1	7.0 ± 1.6	4.7 ± 1.9	2.1 ± 0.8	2.4 ± 0.6	3.1 ± 1.7	3.7 ± 0.7
Sy	em[d]	em[d]	2.4 ± 1.5	em[d]	10.1 ± 3.0	6.0 ± 2.1	5.5 ± 1.7	3.0 ± 1.4	4.2 ± 0.8
LINER[c]	...	...	3.8 ± 2.0	...	14.4 ± 4.9	6.3 ± 2.2	6.4 ± 1.3	4.3 ± 0.6	4.3 ± 0.1
Composite	12.6 ± 5.1[c]	14.7 ± 4.6[c]	5.2 ± 1.6[c]	9.4 ± 2.4[c]	6.3 ± 1.5	3.3 ± 0.4	4.6 ± 0.7	3.3 ± 1.0	4.4 ± 0.6
Hs[b]	9.4 ± 0.8	14.3 ± 2.9	4.0 ± 0.8	6.4 ± 0.6	8.2 ± 0.5	4.0 ± 1.0	5.5 ± 1.1	4.2 ± 1.0	5.0 ± 0.3
N1433	...	...	...	...	11.8	6.9	7.0	3.6	5.0

[a] Only one measurement.
[b] Average of only two measurements.
[c] Average of only three measurements.
[d] In emission.

dance than the previous types as indicated by [N II]/Hα. Several absorption lines in the optical and the Ca II triplet in the near-IR can easily be seen. NGC 7673 shows somewhat larger excitation and no absorption features in the optical and near-IR.

We show in Figure 6 three examples of starbursts: NGC 7714 is the prototype starburst galaxy (Weedman et al. 1981): it is very blue, occurs in a Sdm galaxy, shows high excitation and weak absorption features in the optical and near-IR. NGC 7552 is a red starburst occurring in a SBbc galaxy, showing strong absorption lines in the optical and near-IR, indicating a mixture of moderately young and old red stellar population. The emission spectrum indicates low excitation and high chemical abundance. NGC 5236 presents very similar W of absorption lines and emission-line ratios to NGC 7552, although its continuum is bluer. The difference between the two spectra seems to be due only to reddening effects produced by the different orientation of the galaxies relative to the line of sight (Kinney et al. 1994).

We show in Figure 7 two spectra of composite-type galaxies: the high [O III]/Hβ and [N II]/Hα of NGC 7582 indicates that its emission is dominated by the Seyfert nucleus, while in NGC 1672 the lower ratios indicate that the starburst dominates.

The spectra of the hot spot galaxies are shown in Figure 8: the emission-line ratios are similar to those of the red starbursts, only the equivalent width of the emission lines is smaller, due to a smaller starburst (concentrated in the hot spots). The optical absorption lines indicate that the red underlying population dominates, while in the starbursts there is strong contribution from moderately young stars as shown by the high-order Balmer absorption lines in the spectral region $\lambda\lambda$3700–4000.

Figure 9 shows the spectra of two Seyfert 2 galaxies: notice the high [O III]/Hβ, [N II]/Hα and [S III]/Hα ratios as compared to the previous galaxies. NGC 3081 occurs in a galaxy presenting a red stellar population while IC 3639 shows contribution of blue stars in the absorption spectrum.

Finally, in Figure 10, we present the spectra of the LINERs NGC 4579 and NGC 1433. The two spectra are similar in presenting red stellar populations and a "rising branch" in the UV, as well as low excitation emission lines with relatively small equivalent widths, confirming the classification of NGC 1433 as a LINER.

5. SUMMARY AND CONCLUSIONS

We have presented the spectral energy distributions from the ultraviolet to the near-infrared as well as the measurements of a number of spectral features for a sample of 48 galaxies classified as BCG, H II, starburst, Seyfert 2, and composite (Seyfert + starburst). The spectra were obtained through a matched large ($10'' \times 20''$) aperture. A preliminary analysis of the data was made by grouping the galaxies according to their activity type and calculating average properties. In this section, we summarize the main results.

The Seyfert galaxies present the largest [O III]/Hβ and [N II]/Hα ratios. There is a trend in these ratios from BCDG, through BCG and H II to SBs: [O III]/Hβ decreases while [N II]/Hα increases, which is consistent with a decreasing gas excitation and increasing metallicity. The Hα/Hβ ratio also indicates an increasing reddening along this sequence. The Seyfert galaxies present Hα/Hβ ratios among the highests, although comparable to that of the starbursts, suggesting that we are reaching similar optical depths. We are thus not probing (through the Balmer ratio) the large obscuration frequently found in the Seyfert 2 galaxies through other methods (e.g., Storchi-Bergmann, Wilson, & Baldwin 1992; Schmitt et al. 1994). In our sample, the Seyfert and the starburst galaxies have similar Hα luminosities.

The continuum is bluest for the BCGDs, followed by the BCGs, then the H II's, the SBs, and Sy's. The three LINERs of the sample present the reddest colors.

The equivalent widths of the measured absorption lines in the ultraviolet (Si IV, C IV, Fe II, and Mg II) increase along the sequence from BCDG to starbursts, while in the Seyfert galaxies, these absorption lines are absent, being frequently replaced by emission. In the optical, from the BCDG through the starbursts, the equivalent widths of the measured absorption features (e.g., G band, Mg I and Na I, which originate mainly in the red stars) present small values, indicating the dominance of blue stars in the integrated continuum in these types. The larger values are found for the Seyfert galaxies (except for a few cases) and LINERs, indicating that the old stellar population dominates in these galaxies due to our large aperture.

A more detailed analysis of the data, incorporating both the northern and southern samples is presented in Storchi-Bergmann et al. (1994), Calzetti et al. (1994), and Kinney et al. (1994).

We would like to thank the staff at CTIO for assistance with the observations and reductions, in particular Steve Heathcote, for suggestions about the setups for the observations, and M. Navarrete, for valuable help with the reductions. We are indebted to C. Winge for kindly obtaining some optical spectra for us, and to K. McQuade for preparing the plots. We also benefited from valuable discussions with D. Calzetti, T. Heckman, C. Robert, E. Bica, and C. Bonatto. T.S.B. thanks the hospitality of STScI, where part of this work was done, and the Brazilian institutions CNPq, CAPES, and FAPERGS for partial support. The authors also acknowledge support from the NASA grants NAG5-2498 and NAGW-3757.

REFERENCES

Baldwin, J. A., Phillips, M. M., & Terlevich, R. 1981, PASP, 93, 5
Bica, E. 1988, A&A, 195, 76
Bica, E., & Alloin, D. 1987, A&A, 186, 49
Buta, R. 1986, ApJS 61, 631
Calzetti, D., Kinney, A. L., & Storchi-Bergmann, T. 1994, ApJ, 429, 582
Jones, J. E., Alloin, D., & Jones, B. J. T. 1984, ApJ, 283, 457
Kinney, A. L., Antonucci, R. R. J., Ward, M. J., Wilson, A. S., & Whittle, M. 1991, ApJ, 377, 100

Kinney, A. L., Bohlin, R. C., Calzetti, D., Panagia, N., & Wyse, R. F. G. 1993, ApJS, 86, 5
Kinney, A. L., Calzetti, D., Bica, E., & Storchi-Bergmann, T. 1994, ApJ, 429, 172
Kinney, A. L., Calzetti, D., Bohlin, R. C., McQuade, K., & Storchi-Bergmann, T. 1995, ApJ, submitted
McCall, M. L., Rybski, P. M., & Shields, G. A. 1985, ApJS, 57, 1
McQuade, K., Calzetti, D., & Kinney, A. L. 1995, ApJ, in press
Meurer, G. R., Freeman, K. C., Dopita, M. A., & Cacciari, C. 1992, AJ, 103, 60
Osterbrock, D. E., Tran, H. D., & Veilleux, S. 1992, ApJ, 398, 196
Pagel, B. E., & Edmunds, M. G. 1981, ARA&A, 19, 77
Robert, C., Leitherer, C., & Heckman, T. M. 1993, preprint
Schmitt, H. R., Storchi-Bergmann, T., & Baldwin, J. 1994, ApJ, 423, 237
Sersic, J. L., & Pastoriza, M. G. 1965, PASP, 77, 287
Storchi-Bergmann, T., Bica, E., & Pastoriza, M. G. 1990, MNRAS, 245, 749
Storchi-Bergmann, T., Calzetti, D., & Kinney, A. L. 1994, ApJ, 429, 572
Storchi-Bergmann, T., Wilson, A. S., & Baldwin, J. A. 1992, ApJ, 396, 45
Véron-Cetty, M.-P., & Véron, P. 1986, A&AS 66, 335
Weedman, D. W., Feldman, F. R., Balzano, V. A., & Ramsey, L. W. 1981, ApJ, 248, 105